

# Dual-Axis Tilting Quadrotor Aircraft

An investigation into the overactuatedness thereof



**Nicholas Von Klemperer**

Department of Electrical Engineering  
University of Cape Town  
Rondebosch, Cape Town  
South Africa

**October 2016**

MSc thesis submitted in fulfilment of the requirements for the degree of Masters of Science in the  
Department of Electrical Engineering at the University of Cape Town

*Keywords:* Control, Allocation, Non-linear, Autopilot



# Declaration

I, Nicholas Von Klemperer, hereby:

1. grant the University of Cape Town free license to reproduce the above thesis in whole or in part, for the purpose of research only;
2. declare that:
  - (a) This thesis is my own unaided work, both in concept and execution, and apart from the normal guidance from my supervisor, I have received no assistance except as stated below:
  - (b) Neither the substance nor any part of the above thesis has been submitted in the past, or is being, or is to be submitted for a degree at this University or at any other university, except as stated below.
  - (c) Unless otherwise stated, any and all illustrations or diagrams demonstrated in this work are productions of my own.
  - (d) All the content used to compile this report and complete the investigation revolving around the whole project is collectively hosted on the following GIT repositories:
    - L<sup>A</sup>T<sub>E</sub>Xreport: <https://github.com/nickvonklemp/Masters-Report>
    - STM32F303 Projects: <https://github.com/nickvonklemp/Code>
    - Design Files & Blue Prints: <https://github.com/Design>
    - Hardware Schematics: <https://github.com/nickvonklemp/visio> &
    - EagleCad Schematics <https://github.com/nickvonklemp/Eagle>
    - MatLab Simulink Code: <https://github.com/nickvonklemp/Simulink>
    - Results & Simulation Data: <https://github.com/nickvonklemp/results>

---

Nicholas Von Klemperer  
Department of Electrical Engineering  
University of Cape Town  
Thursday 13<sup>th</sup> October, 2016

# Abstract

## Dual-Axis Tilting Quadrotor Aircraft

Nicholas Von Klemperer

Thursday 13<sup>th</sup> October, 2016

The aim of this project is to design, simulate and control a novel quadrotor platform which can articulate all 6 Degrees of Freedom by vectoring the propeller's directional thrust. To achieve this the structure of the air-frame must redirect those thrust vectors to any desired orientation. This means it has to transform its configuration during flight, redirecting lift actuators whilst still maintaining stable attitude & position control, despite of such relative motion. In view of this required articulation the proposal is to add 2 axes (degrees) of extra actuation to each propeller. As a result each lift propeller can then be pitched or rolled relative to the body frame. This adaptation, to what is an otherwise well covered and highly researched platform, produces an over-actuated control problem. Actuator allocation is the primary contribution of this paper with novel elements of non-linear (*state-space*) attitude control and plant uncertainty compensation.

The structure of the dissertation first presents the design which the subsequent dynamics and control are derived with respect to. Following that, the kinematics associated with rigid bodies are derived. Any unique effects that could apply to the design like gyroscopic, inertial and aerodynamic responses are investigated and then incorporated into the dynamics. Position and control algorithms are first derived, then simulated and compared based on the plant's dynamics (*which include discretionary effects on the system*). The relative performance of the controllers are evaluated but regular performance metrics for attitude and position control are ill-suited for such a system. Some time is spent discussing the consequence of this and how the controllers are actually evaluated. Finally the design is built and tested using readily available RC components and conclusions drawn on the success or failure of the design.

The purpose of the investigation is the practicality and feasibility of such a design, most importantly whether the complexity of the mechanical design is a decent compromise for the added degrees of control actuation. The outcome of the build is to ascertain if it's both economically (cost and control effort) feasible to use such a prototype to expand the range of a quadrotor's motion. The design and control treatment presented here are by no means optimal nor the most exhaustive solutions, focus is placed on the system as a whole and not just one aspect of it.

*This dissertation report is presented in a logical progression of concepts and information. In some cases the research and results were compiled differently from how they're listed.*

# Acknowledgements

# Nomenclature

Propeller Rotational Speed:  $\Omega_i$  [rpm]

*Rotational speed in RPS is used for Blade Element Theory Calculations in Chapter:3*

Inertial Position:  $\vec{P} = [X_I \ Y_I \ Z_I]^T \in \mathcal{F}^I$

Body Position:  $\vec{E} = [x \ y \ z]^T \in \mathcal{F}^b$

Euler Angles:  $\vec{\mathcal{E}} = [\phi \ \theta \ \psi]^T$

# Contents

<b>Declaration</b>	<b>ii</b>
<b>Abstract</b>	<b>iii</b>
<b>Acknowledgements</b>	<b>iv</b>
<b>Nomenclature</b>	<b>v</b>
<b>1 Introduction</b>	<b>1</b>
1.1 Foreword . . . . .	1
1.1.1 A Brief Background to the Study . . . . .	1
1.1.2 Research Questions & Hypotheses . . . . .	2
1.1.3 Significance of Study . . . . .	2
1.1.4 Scope and Limitations . . . . .	3
1.2 Literature Review . . . . .	6
1.2.1 Existing & Related Work . . . . .	6
1.2.2 Notable Quadrotor Control Implementations . . . . .	9
<b>2 Prototype Design</b>	<b>13</b>
2.1 Conventions Used . . . . .	13
2.1.1 Reference Frames Convention . . . . .	13
2.1.2 Motor Axis Layout . . . . .	15
2.2 Design . . . . .	17
2.2.1 Actuation . . . . .	17
2.2.2 Inertial Matrices & Mass . . . . .	20
2.3 System Layout . . . . .	25
2.3.1 Actuator Transfer Functions . . . . .	28

<b>3</b>	<b>Kinematics &amp; Dynamics</b>	<b>29</b>
3.1	Rigid Body Dynamics . . . . .	29
3.1.1	Lagrange Derivation . . . . .	29
3.1.2	Rotation Matrix Peculiarities . . . . .	30
3.1.3	Quaternion Dynamics . . . . .	30
3.1.4	The Unwinding Problem . . . . .	30
3.2	Non-linearities . . . . .	30
3.2.1	Gyroscopic Torques . . . . .	30
3.2.2	Coriolis Acceleration . . . . .	30
3.2.3	Inertial Matrix . . . . .	30
3.3	Aerodynamics . . . . .	30
3.3.1	Thrust Forces & Propeller Torques . . . . .	30
3.3.2	Drag . . . . .	30
3.3.3	Conning & Flapping . . . . .	30
3.3.4	Vortex Ring State . . . . .	30
3.4	Consolidated Model . . . . .	30
<b>4</b>	<b>Control Treatment</b>	<b>31</b>
4.1	Attitude Control . . . . .	32
4.1.1	The Attitude Control Problem . . . . .	32
4.1.2	Quaternion Based Controllers . . . . .	32
4.1.3	Non-linear Controllers . . . . .	32
4.2	Position Control . . . . .	32
4.2.1	Backstepping Position Controller . . . . .	32
4.3	Controller Allocation . . . . .	32
4.3.1	Non-linear Plant Control Allocation . . . . .	32
4.3.2	Pseudo Inverse Allocator . . . . .	32
4.3.3	Weighted Pseudo Inverse Allocator . . . . .	32
4.3.4	Priority Norm Inverse Allocator . . . . .	32
4.3.5	Online Optimized Secondary Goal Allocator . . . . .	32
<b>5</b>	<b>Simulations &amp; Results</b>	<b>33</b>



5.1	Controller Tuning . . . . .	33
5.1.1	Partical Swarm Based Optimization . . . . .	33
5.1.2	Performance Metric . . . . .	33
5.1.3	Global & Local Minima . . . . .	33
5.1.4	Fmincon Differences . . . . .	33
5.2	Simulation Block . . . . .	33
5.3	State Estimation . . . . .	33
5.4	Optimized Controller Comparisons . . . . .	33
5.4.1	Allocator Performance . . . . .	33
5.4.2	Attitude Control Results . . . . .	33
5.4.3	Autopilot Outcome . . . . .	33
<b>6</b>	<b>Prototype Flight Results</b>	<b>34</b>
<b>A</b>	<b>Standard Quadrotor Dynamics</b>	<b>35</b>
<b>B</b>	<b>Design Bill of Materials</b>	<b>36</b>
B.1	Parts List . . . . .	36
B.2	F3 Deluxe Schematic Diagram . . . . .	41
<b>C</b>	<b>System ID Test Data</b>	<b>42</b>
C.1	Servo Data . . . . .	42
C.2	Cobra CM2208-200KV . . . . .	43
<b>D</b>	<b>Full Equations</b>	<b>44</b>
D.1	Inertias . . . . .	44

# List of Figures

1.1	.....	5
1.2	General Structure for Opposed Tilting Platform . . . . .	6
1.3	DJI Inspire 1 . . . . .	7
1.4	.....	8
1.5	Dual-axis tilt-rotor mechanism . . . . .	9
1.6	ArduCopter PI Euler Angle Attitude Control loop . . . . .	10
2.1	Inertial and Body Reference Frames . . . . .	13
2.2	Aligned Motor Frame Axes . . . . .	15
2.3	Intermediate Motor Frames . . . . .	15
2.4	Body Frame Axes Layout . . . . .	16
2.5	Isometric layout of the designed prototype . . . . .	17
2.6	Motor Assembly . . . . .	18
2.7	Difference between propeller and motor planes . . . . .	18
2.9	Corona Servo Bracket . . . . .	19
2.10	Inertial Measurement References . . . . .	20
2.11	Body Frame Center of Mass . . . . .	22
2.12	Inertial Center & Mass Center . . . . .	23
2.13	Hardware Schematic Diagram . . . . .	25
2.14	SPRacing F3 Deluxe Flight Controller . . . . .	26
2.15	S.BUS Data Stream . . . . .	26
2.16	.....	27
B.1	Bearing Bracket Inner Ring Assembly . . . . .	38
B.2	Servo Bracket Inner Ring Assembly . . . . .	38

B.3	Servo Bracket Middle Ring Assembly . . . . .	38
B.4	Bearing Holder Middle Ring Assembly . . . . .	38
B.5	Servo Mount Middle Ring Assembly . . . . .	38
B.6	Bearing Shaft Middle Ring Assembly . . . . .	38
B.7	Bearing Holder Damping Assembly . . . . .	39
B.8	Servo Mount Damping Assembly . . . . .	39
B.9	Servo Mount Damping Bracket . . . . .	39
B.10	Bearing Holder Damping Bracket . . . . .	39
B.11	Arm Mount Damping Bracket . . . . .	39
B.12	Frame Brackets . . . . .	39
B.13	F3 Deluxe Flight Controller Hardware Schematic . . . . .	41
C.1	Official Test Results for Cobra Motors . . . . .	43

# List of Tables

1.1	A Breakdown of common Attitude Controllers . . . . .	10
2.1	Analogue & Digital Timing Signals . . . . .	19
B.1	Parts List . . . . .	36
B.2	3D Printed Parts . . . . .	37
B.3	Inner & Middle Ring Assemblies . . . . .	38
B.4	Damping Assemblies . . . . .	39
B.5	Laser Cut Damping Brackets . . . . .	39
B.6	Laser Cut Parts . . . . .	40

# Chapter 1

## Introduction

### 1.1 Foreword

#### 1.1.1 A Brief Background to the Study

A popular topic for current control and automation research is that of quadrotor UAVs. Attitude control of a quadrotor poses a unique 6-DOF control problem, to be solved with an under-actuated 4-DOF system. As a result the  $\phi$  pitch and  $\theta$  roll plants aren't directly controllable. The attitude plant is often simplified around a stable operating point. The trimmed operating region is always at the inertial frame's origin; resulting in a zero-set point tracking problem. The highly coupled non-linear dynamics of a rigid body's translational and angular motions arise from gyroscopic torques [Section: 3.2.1] and Coriolis accelerations [Section: 3.2.2]. These effects are negligible around the origin<sup>1</sup>, hence the origin trim point removes the system's nonlinearities. The control system can then reduce each state variable,  $\vec{X}_b = [\phi \ \theta \ \psi \ x \ y \ z]^T$ , to individual SISO plants.

As almost every recent quadrotor research paper mentions, the late interest in the platform is from recent emergences in availability of MEMS systems and low-cost microprocessors. Such advancements accommodate onboard state estimation and control algorithm processing in real time. Developmental progress in quadrotors and, to a lesser extent, UAVs in general has led to rapidly growing enthusiast communities. HobbyKing [34] is now synonymous with providing custom DIY hobbyist quadrotor kits, not just prebuilt commercial products like the DJI Phantom [21].

The avenue for potential application of both fixed wing and VTOL UAVs is expansive, supporting civil [59], agricultural [62] and security [44] industries. The quadrotor platform provides a mechanically simple platform on which to test advanced aerospace control algorithms. Commercial drone use in industry is already emerging as a prolific sector; especially in Southern Africa. Subsequently following the 8<sup>th</sup> amendment of civil aviation laws [65], commercial use of UAVs is now both legal and regulated. Research into any non-trivial aspect of the field will therefore be to extremely valuable to the field as a whole.

Large scale quadrotor, hexrotor and even octotoror UAVs are popular intermediate choices for aerial cinematography due to their high payload capacity. The cost of a commercial drone like the SteadiDrone Maverik [49] is far less than a chartered helicopter used for the same panoramic aerial scenes or on-site inspections. One foreseeable issue which may hinder commercial drone progress in the agricultural and civil sectors is the consequential inertial effects from scaling up the aerospace bodies. When scaling up any vehicle, its performance is adversely affected if actuation rates aren't proportionately scaled.

---

<sup>1</sup>Expanded upon in Appendix:A

### 1.1.2 Research Questions & Hypotheses

The difficulty with quadrotor control is that fundamentally it's unstable and under-actuated, *empirically proven later with Layupanov Theorem in Chapter:4*. A quadrotor only has four controllable inputs, namely propeller rotational speeds,  $\Omega_{1,2,3,4}$ , which are then abstracted<sup>2</sup> to virtual control inputs net torque,  $\vec{\tau}_{net} = [\tau_\phi \ \tau_\theta \ \tau_\psi]^T$ , and a perpendicular heave thrust  $\vec{T}_{net} = \sum_{i=1}^4 T(\Omega_i)$ . Those four inputs have to affect both the linear X-Y-Z positions,  $P = [x \ y \ z]^T$ , and angular pitch, roll and yaw rotations,  $\mathcal{E} = [\phi \ \theta \ \psi]^T$ . Pitch and roll torques,  $\tau_\phi$  &  $\tau_\theta$ , are induced from differential thrusts of each opposing propeller. Yaw torque,  $\tau_\psi$ , is dependent on net aerodynamic torque about the rotational axes of each propeller (See Section:3.3.1). Aerodynamic responses are non-linear and fluctuating sources of control torques and as such the body's yaw control is depreciated. A result of the under-actuation is that the attitude control problem then becomes a zero set point problem, any other attempt to track attitude cannot be achieved.

The aim of this project is to implement quadrotor attitude and position set point tracking by solving the problem of its inherent under-actuation. Inspired by Boeing/Bell Helicopter's V22 Osprey and the tilting articulation of its propellers, the prototype design proposed here introduces two additional actuators for each of the quadrotor's lift propellers. Specifically, adding rotations about the X and Y axes for each motor/propeller pair. The result is a vectored 3 dimensional thrust force rather than a bound perpendicular heave thrust. The control problem is then posed as the design of net forces,  $\vec{F}_{net} = [F_x \ F_y \ F_z]^T$ , and torques,  $\vec{\tau}_{net} = [\tau_\phi \ \tau_\theta \ \tau_\psi]^T$ , for a general 6-DOF body such that for any given trajectory,  $X_d = [x \ y \ z \ \psi \ \theta \ \phi]^T$ , the error state  $X_e = X_d - X_b$  asymptotically tends to  $\vec{0}$ .

$$\lim_{t \rightarrow \infty} X_e = \vec{0} \quad \forall X \in \mathbb{R}^n \quad (1.1)$$

Where  $n$  is the degrees of freedom. The over-actuation brings about the need for a control allocation scheme which distributes the 6 commanded system inputs (net torques and forces) among the actuator set (12 actuators) in order to optimize some objective function secondary to that of Eq:1.1.

Part of the control research question is the multivariable treatment of the system, making no assumptions or simplifications to the non-linear dynamics involved in the quadrotors motion and its operational conditions. Standard linearizations applied to the quadrotor's control plant won't hold true for the more aggressive manoeuvres; they're dependent on small angle approximations and negligible  $2^nd$  order effects. Stable control law design will need to expand and simulate the existing kinematic model of an aerial body and apply it to a quadrotor's motion. Following this there must be design, development and control of the new actuator suite which is to be implemented on a quadrotor platform. Final key outcomes for the project are the simulation analysis and prototype construction for the proposed design and the conclusion drawn thereon.

Introducing relative motion within an unconstrained body will produce a lot of unwanted dynamics like inertial and gyroscopic responses, amongst others. A rotating propeller will respond to pitching much like a Control Moment Gyroscope [87] or a flywheel and produce a precipitating torque. A less trivial aspect to consider is the aerodynamic torque produced from the propeller's aerofoil profile. Such induced responses occur in planes perpendicular to whatever the propeller's rotation exists in. These aspects are normally compensated for due to a quadrotor's fundamental co-planar propeller rotation. It's anticipated that a plant dependent control solution will have to compensate for these dynamics, which if left unaccounted for could potentially cause instability.

### 1.1.3 Significance of Study

Due to the huge popularity of quadrotor platforms as research tools, any work that improves the UAV & quadrotor general body of knowledge will prove to be valuable. With that being said, there

---

<sup>2</sup>The abstraction of which is explored in Appendix:A

is already a vast amount of existing research on linear and non-linear control techniques for regular quadrotor platforms. The attitude loop is the most common topic for control research, requiring an under-actuated solution and mostly linearized around the origin (See Appendix:A). Far less common is the application of optimal flight path and trajectory planning to quadrotor control. The uniqueness and difficulty of the quadrotor attitude control does not hold true for its position control, so standard techniques can be used for way point planning and the like once the attitude control problem has been solved.

The most significant aspect of this project is the attitude control, discussed later in Section:4.1. The over-actuation of the proposed design and, more critically, the manner in which the controller's (virtual) output is distributed among those control effectors would appear to be the first of its kind. Otherwise known as control allocation, the requirements of the distribution algorithm(s) are outlined in Section:4.3. Dynamic set point attitude control for aerospace bodies is not a subject heavily researched outside the field of satellite attitude control. Even papers which propose similarly complex mechanical over-actuation (expanded upon in next in the literature review, Section:1.2) hardly broach the topic of tracking attitude set points away from the origin.

Whilst the control plant (developed in Chapter:4) does indeed close both the position and attitude control loops, there is no consideration of trajectory generation nor flight path planning. Such topics are well discussed elsewhere in a far more concise and deliberate way than this project could ever hope to achieve. Once closed loop position and attitude control has been achieved, the control algorithms can be adjusted to account for higher order state derivative (acceleration, jerk and jounce) tracking needed for nodal way point planning. The heuristics involved with flight path planning are well documented and their implementation is an academic task.

Where possible the system identification and control (design and allocation) for this project is kept both modular and generically applicable. The intention here is that its pertinence falls not only within the UAV field but to any aerospace or free body attitude control. Hopefully this investigation can be expanded upon with more in-depth research on one of the subsystems without compromising the stability of the remainder of the whole plant.

Provisionally, an obvious outcome which the investigation could yield is improved yaw control of a quadcopter's attitude. However, if the express purpose was just to improve yaw control, it could be done with a dramatically more simple design. Furthermore, the project could provide greater insight into high bandwidth actuation and thus a faster control response for larger aerospace bodies. Any standard quadrotor uses differential thrust to develop a torque about its body. Such actuation suffers a second order inertial response when the propellers accelerate or decelerate,  $\tau_{simplified} = \mathbb{I}_f \dot{\omega}_i$ . Prioritizing pitching the propeller's principle axis of rotation rather than changes to the propeller's speed could potentially improve the virtual control response. This is entirely dependent on how the allocator block is prioritized (presented in Section:4.3).

### 1.1.4 Scope and Limitations

#### Scope

Critical to this project is the conceptualized design and prototyping of a novel actuation suite to be used on a quadrotor platform. The express purpose of which is to apply set point attitude tracking control to the body. Stemming from this is an investigation into the kinematics that are potentially influenced by the design and the structure's relative motion. In order to apply correct control theory to achieve the attitude tracking on a physical prototype, the plant dynamics must first be identified for input responses to be approximated with confidence. Aspects of the mechanical design are covered next in Section:2.2 but, beyond the cursory investigation, there is no scope for materials analysis or stress testing of the design. To the detriment of the project, the design will either produce an over-

engineered or catastrophically under-engineered solution. The scope focuses mainly on the control application and embedded systems design, not the structural integrity of a proposed frame given the forces it may undergo. Physical measurements are only made for critical kinematics, such as inertial measurements for the second order gyroscopic and inertial dynamic responses.

As mentioned in the antecedent Section: 1.1.3, trajectory & flight path planning are not ubiquitous with this dissertation. Derivations for the differential equations which dictate a 6-DOF body's movement are wholly applicable to any dynamic (rigid or otherwise) aerospace body, although some particular standards are used [sic Z-Y-X Euler Aerospace Sequence, Section:2.1]. Similarly the control plant is stabilized with non-linear state space control techniques, aided and justified by Lyapunov theorem. Alternative solutions through Model Predictive Control or Quantitative Feedback Theory could provide more refined or effective controllers, they aren't presented and remain open to further investigation. Quadrotor attitude control is commonly stabilized with feedback linearizations, decoupling plant around a trim point so that SISO techniques can be applied. A derivation of such a linearization is included in Appendix:A but beyond that there are no further discussions. Any comparison between non-zero and zero-set point attitude control of quadrotor is difficult as the fundamental objectives are in stark contrast with one another.

Arguably the most important and indeed novel aspect of this project is the control allocation. The system has 12 plant inputs and 6 output variables to be controlled. There is then a family of actuator set  $u \in \mathcal{U}$  solutions that exist for each commanded input. Such a plant is classified as over-actuated. Ergo, there must be some logical process as to how those 12 inputs are articulated to achieve the desired 6 movements. Appropriate techniques are first investigated in Section:4.3 and compared before a final solution is implemented in Section:5.4. It is by no means a comprehensive investigation of every possible allocation scheme but rather an analysis of the sub-set of problems and design of what is regarded as a logical and pertinent approach.

With regards to the actual prototype design, in Section 2.2, it's assumed that certain aspects are a given certainty. Particularly the state estimation, updated through a 4-camera positioning system fused with a 6-axis IMU through Kalman Filtering, is assumed to be precise and readily disposable at a consistent 50 Hz. Hence state estimation is included but is bereft of intricate detail, this is another topic which remains open to further investigation.

## Limitations

The biggest constraint faced by the design is the net weight of the assembled frame. Lift forces required to keep the body aloft are obviously dependent on the all up weight. Conventional wisdom has it that steady state actuator rates ought to be far less than saturation conditions. For stability to be guaranteed at all feasible operating conditions, the actuators must have sufficient headroom to still effect the desired control inputs. Conversely the structure's net weight is mostly dependent on the lift motors, often being the heaviest part of the vehicle (*batteries too*). A trade-off between net weight and actuator efficacy makes designing the prototype a balancing act of compromise; added actuation is needed to produce the desired thrust vectoring. That added actuation is going to increase the weight which then requires more thrust force to ensure the vehicle remains airborne. Larger motors then need stronger actuators to effect the relative motion and overcome the bodies inertial response. It's a compromise between the weight of the body and the strength/quality of the actuation.

To forego the deliberation detailed above, reducing the possibility of unbounded scope creep, a limitation is self-imposed on the prototype design. Restricting the propeller diameter, and hence maximum thrust, will provide a constraint upon which all other design considerations must conform. Smaller propellers require a far greater rotational to produce a similar level of thrust as their larger diameter counterparts. Electing to use 3 blade 6X4.5 inch small diameter propellers is going to reduce the overall dimensions of the prototype, but as a consequence will require very high RPM motor. Specifically



a set of four Cobra-2208/2000KV [18] Brushless DC motors are be used for lift actuation. A direct consequence of this decision is that, provisionally based upon test data<sup>3</sup>, the net thrust disposable for actuation is limited to around 950g,  $\approx 9$  N, per motor (see Section:3.3.1). It's critical to ensure the control block doesn't induce over-saturation of the motor actuation, so the frame weight needs to be around 50-60% of the maximum available thrust, or roughly 2 Kg. Saturation conditions are detailed later in Section: 4.3.

Another aspect of limitations produced by design decisions made, mostly to reduce prototype costs and weight, is to use of 180° rotation servo motors. The servos are for individual motor's  $\vec{X}_{M_i}$  and  $\vec{Y}_{M_i}$  axial pitch and roll actuations respectively. The servos act in lieu of either continuous BLDC or stepper motors. Any non-servo rotations beyond 360° will require closed loop position control and, unlike servos, would need slip rings to transmit power throughout rotational movement. However the logistics of implementing such a design whilst maintaining an acceptable weight is almost impossible. Such an implementation is going to dramatically scale up the size of the prototype to accommodate for weight increases. Commercial camera stabilizing gimbals already make use of similar configurations but the I/O requirements from the flight controller  $\mu C$  already constricts the amount of expansion available.



(a) Cobra CM2208/2000KV BLDC Motor



(b) Corona DS-339MG Digital Servo

**Figure 1.1**

Discrete elements for the whole system can potentially limit performance but are going to be mitigated if possible. For example analogue servos have an associated 1ms deadband from their 20Hz refresh rate. That can be addressed by using faster, albeit more expensive, digital servos which samples at 330Hz. The prototype's flight controller has to provide 12 PWM output compare channels for the 8 servos and 4 BLDC speed controllers. State updates from a ground control station and a fail safe 6Ch RC receiver module also needs to be processed by the  $\mu$ controller system. Particular attention is paid to the embedded system layout in Section:2.3.

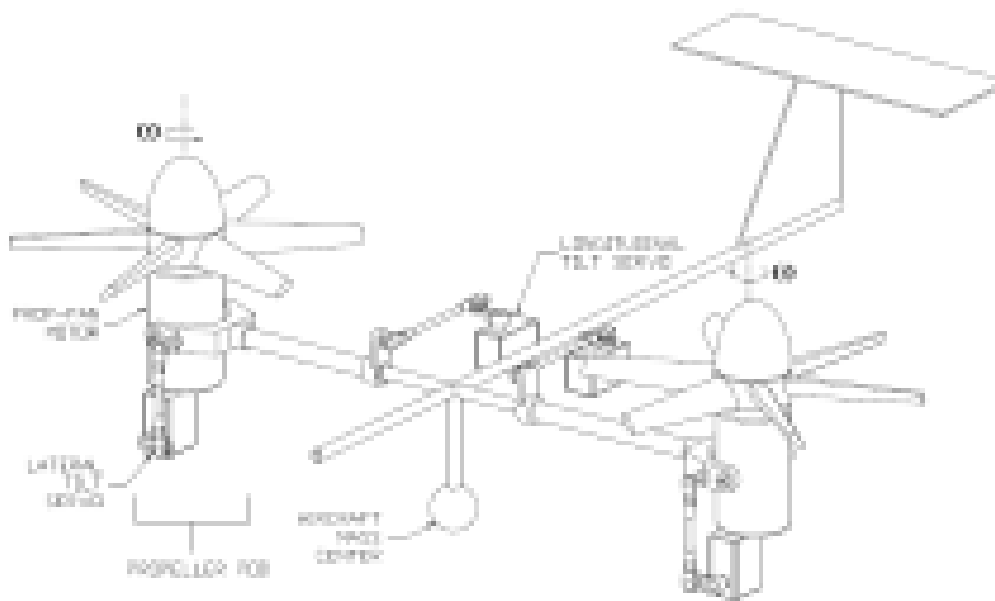
<sup>3</sup>Official test data from [18] included in Appendix:C.2 and tested independently in Section:3.3.1

## 1.2 Literature Review

### 1.2.1 Existing & Related Work

The field of transformable aerospace frames is not necessarily a new one, with many commercial examples having seen a lot of success over their operational life span. The most notable tilting-rotor vehicle is that of the Boeing/Bell V22 Osprey <sup>4</sup> aircraft. First introduced in the field in 2007, the Osprey has the ability to pitch its two lift propellers forward to aid translational flight after vertically taking off or landing. In addition to this there have been a few papers published on similar tilting bi-rotor UAVs for research purposes.

#### Biorotors



**Figure 1.2:** General Structure for Opposed Tilting Platform

Research into birotor vehicles (Fig:1.2)<sup>4</sup> with ancilliary lift propeller actuation is oft termed Opposed Active Tilting or *OAT*. Such a rotorcraft’s mechanical design applies either a single *oblique*  $45^\circ$  tilting axis relative to the body; [8, 28, 40], or a *lateral* tilting axis, adjacent to the body; [15, 41, 61, 75]. Leading research is currently focussed on applying doubly actuated tilting axes to birotor UAVs. Dual axis Opposed Active Tilting or *dOAT* introduces vectored thrust with propeller pitch and roll motions to further expand the actuation suite, [2, 27]. A birotor is sometimes considered preferable to the multirotor platform due to its reduced controller effort. However the controller plant abstraction often detracts from the quality and effectiveness of its stability solution as a result of the birotor’s underactuation.

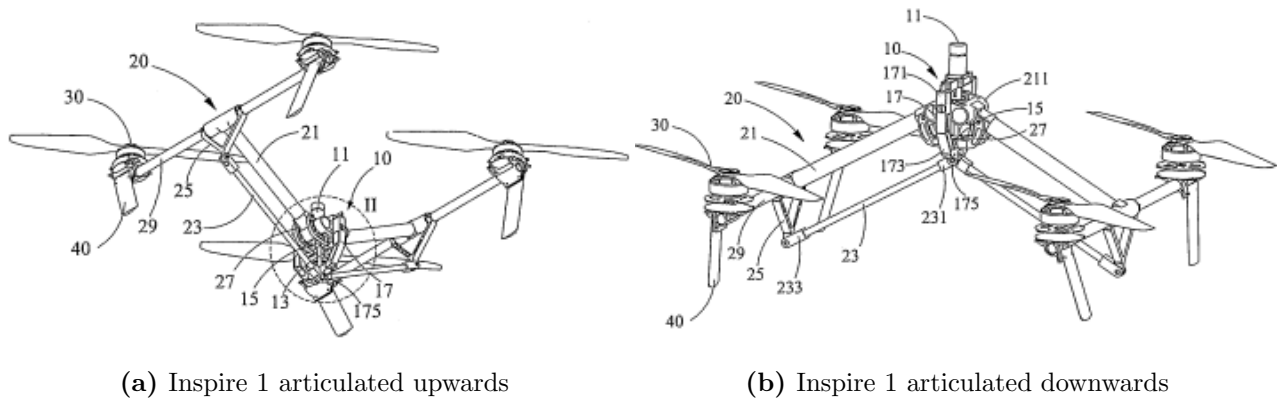
Birotor attitude control typically incorporates plant independent PD [8] and PID [61] controller schemes. Occasionally more computationally exhaustive and plant dependent Ideal and Adaptive backstepping controllers (*IBC* or *ABC*) are exploited, presented in [40, 75] and [41] respectively. The cross-coupling of a birotor vehicle’s attitude system is more pronounced than that of a quadrotor, derived in Section:3.2, and so feedback linearisation is almost always used. In an interesting progression from the norm, Lee et al, [46], proposed a PID co-efficient selection algorithm for a bi-rotor control block. Using a Particle Swarm Optimization technique, similar to [89], the coefficients were globally optimized around a given performance metric. However their performance criterion is a basic

<sup>4</sup>Image from G. Gress: [27]

ITAE<sup>†</sup> term and nothing more appropriate involving effects unique to flight systems. *PSO* algorithms iteratively search for a globally optimized solution and offer independent, derivative free optimization. Later on non-linear controller coefficient are also optimized here using a *PSO* algorithm, shown in Section:5.1.

## Quadrotors

Expanding on multirotor vehicles, the quadrotor UAV is a popular and well researched platform due to its mechanical simplicity. What would appear to be one of the first quadrotor research implementations, in 2002, is the X4-Flyer quadrotor, [30, 67]. Alternative iterations like the Microraptor [70] and STARMAC [35] quadcopters have subsequently been built and tested. A plethora of literature exists around quadrotor kinematics & control [4, 11, 17, 50, 69], however dedicated rigid body 6-DOF dynamic papers [52, 63] provide better explanations of the kinematics. Often the plant's dynamics are simplified around an origin trim point and assumed to reduce into 6 SISO plants for each degree of freedom (Appendix:A). Lately research projects have begun to incorporate aerodynamic effects like drag and propeller BEM theory into the plant model [13, 35, 72]. Although mostly negligible under standard operating conditions, the higher fidelity models offer more precision without linearisations or assumptions, [5, 35].



**Figure 1.3:** DJI Inspire 1

At the time of writing, the only commercial example of a transforming quadrotor is the DJI Inspire1 [20], made by Shenzhen DJI Technologies (better known for the hugely successful DJI Phantom drone [21]). The Inspire can articulate its supporting arms up and down as shown in Fig:1.3<sup>5</sup>. The aim of such movements is to both alter the center of gravity and further expose a belly mounted camera gimbal for panoramic viewing angles. This transformation changes the moment of inertia about the body's center of gravity, in turn changing the inertial torque response induced by angular movements, an otherwise detrimental effect which makes researchers apprehensive of transformable aerospace frames. The range of transformations which the frame can undergo is limited to just articulating the arms up and down.

In a similar fashion to the progression seen in birotor state-of-the-art, quadrotor research is engaging the topics of single and dual axis tilting articulations. First conceptualized and implemented on a prototype related to an ongoing project covered in two reports, [73, 74]. The authors M. Ryll et al.(2012, 2013) modified and tested a QuadroXL four rotor helicopter, produced by MikroKopter [25], to actuate a single axis of tilting aligned with the frame's arms (Fig:1.4a)<sup>6</sup>. Their proposed control solution, discussed in detail next in Section:1.2.2, assumes no nominal linearised conditions around hover flight, unlike a similar single axis tilting quadrotor prototype designed by Nemati, et al. (2012) [57]. The latter remains simulated but as yet untested.

<sup>5</sup>Both images were sourced from the drone's patent, held by SZ DJI Tech Co [88]

<sup>6</sup>Image sourced from Modelling and Control of a Quadrotor UAV with tilting propellers, [73]

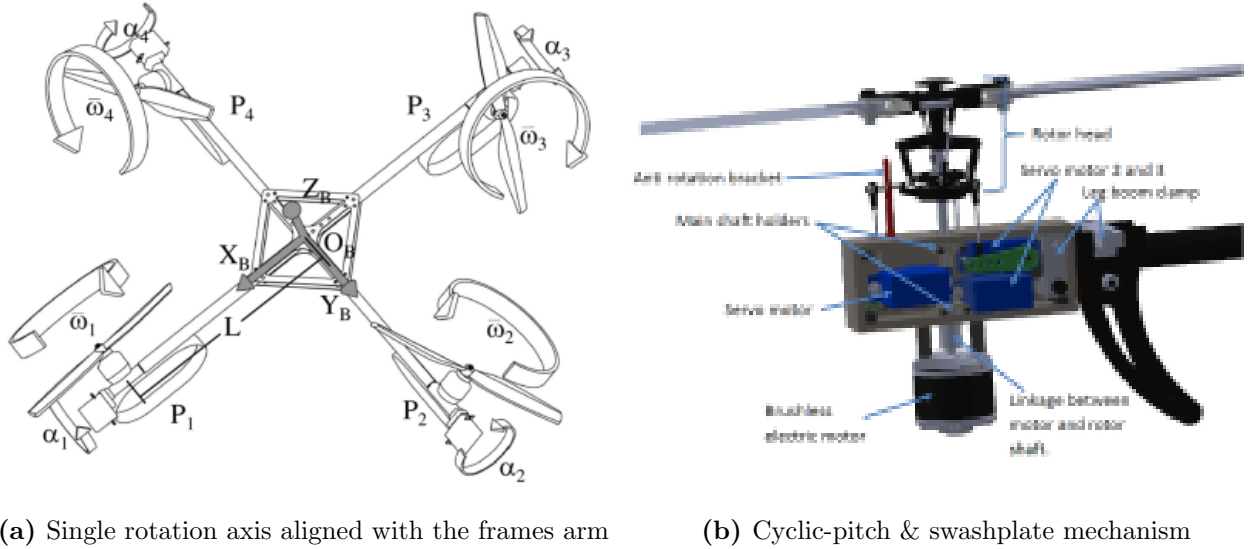


Figure 1.4

One approach to improving quadrotor flight response is to alter the manner in which the thrust is mechanically actuated, potentially improving the actuator bandwidth. Drawing from helicopter design, a project by Napsholm, (2013) [56], purported a quadrotor UAV prototype that used swashplates for varying the propeller pitch and generating torque moments. The aim was a design which wasn't dependent on speed control (*ESC*) power electronics to actuate variable thrust forces. Petrol motors were intended for use in place of BLDC motors. Furthermore, the design proposed a single axis of tilt actuation to each of the four motor modules. Whilst mechanically complex, Napsholm made use of existing RC helicopter components to design a rotor actuation bracket (Fig:1.4b). The cyclic-pitch swashplate used [58] could apply torques,  $\tau_\phi$  and  $\tau_\theta$ , about the propeller's hub, *principle axis of rotation*, by altering the blades angle of attack throughout its rotational cycle. The actuation rate of such a configuration is far faster than that of a differential torque produced rolling/pitching motion.

Irrespective of the strong initial design in the early stages of his project, it would appear that Napsholm's research suffered due to time constraints. The introductory derivation on aerodynamic effects and deliberation over the design provide clear insight into the projects goals. However the control solution and system architecture, electronic and software, are significantly lacking. An introductory proposal of an MPC attitude control system detracted from the comprehensive dynamics discussed. The project ended before testing, simulation and results could be obtained. Unfortunately, despite the novel over-actuated design, there was no discussion given on how the allocation, being the most unique aspect, would be performed.

Finally, the most crucial research to mention is a project completed by Pau Segui Gasco [24], which was a dual presented MSc project with Yazan Al-Rihani [1]. At the time of writing, this would appear to be the only project published pertaining to *over-actuation* in aerospace bodies implemented on a quadrotor platform. The research was split between the two authors who completed the control/electronic design and the mechanical design for their respective MSc dissertations. Shown in Fig:1.5<sup>7</sup>, the dual-axis articulation is achieved using an RC helicopter tail bracket and servo push-rod mechanism; reducing the mass of the articulated component but limiting the range of actuation. Considering the propellers as a spinning flywheel, the induced gyroscopic response can then be treated as an actuator plant. The commanded virtual control is then distributed by weighted inversion among the actuator set, Section: 1.2.2. The whole project justifies the extra actuation as redundancy but doesn't necessarily prove how such a redundancy could be beneficial.

<sup>7</sup>Image from Development of a Dual Axis Tilt Rotorcraft UAV: Modelling, Simulation and Control [24]



Figure 1.5: Dual-axis tilt-rotor mechanism

### 1.2.2 Notable Quadrotor Control Implementations

#### Quadcopter Attitude Control

Attitude control of a 6-DOF body is best described by *The Attitude Control Problem* [82]. A rigid body that currently has an attitude state<sup>8</sup>  $\vec{\mathcal{E}}_s$  and a desired state  $\vec{\mathcal{E}}_d$ , the problem is to then find a torque control law:

$$\mu\tau = h(\vec{\mathcal{E}}_s, \vec{\mathcal{E}}_d, \dot{\vec{\mathcal{E}}}_s, \dot{\vec{\mathcal{E}}}_d) \quad (1.2)$$

Such that both the angular position  $\lim \vec{\mathcal{E}}_s \rightarrow \vec{\mathcal{E}}_d$  and that angular rates  $\lim \dot{\vec{\mathcal{E}}}_s \rightarrow \dot{\vec{\mathcal{E}}}_d$  asymptotically stabilize as  $t \rightarrow \infty$ . A distinction must be made between angular rate vector,  $\dot{\vec{\mathcal{E}}} = [\dot{\phi} \ \dot{\theta} \ \dot{\psi}]^T$  and the angular velocity vector  $\vec{\omega}_b = [p \ q \ r]^T$ . Depending on how the attitude is posed; with rotation matrices [43, 52, 63], quaternions [23, 26, 29, 43] or otherwise (Direct Cosine Matrix etc ...) the error state<sup>9</sup>  $\Delta\vec{\mathcal{E}} = \vec{\mathcal{E}}_d - \vec{\mathcal{E}}_s$  could then differ to a (hamilton) multiplicative relationship. Note that here  $\vec{\mathcal{E}}$  is not necessarily an Euler set but any attitude representative state variable. Simulation and modelling papers often rely on Euler angle based rotation matrices for attitude representation, [10, 11, 51, 57, 71] without addressing the inherent singularity associated with such an attitude representation (sic Gimbal Lock, [76], Section:3.1.2). The alternative quaternion attitude representation, first implemented on a quadrotor UAV in 2006 [80], is often used in lieu of rotation matrices but has its own caveat of *unwinding*, (Section:3.1.4), as a result of quaternions dual-coverage [54] in  $\mathbb{R}^3$  space.

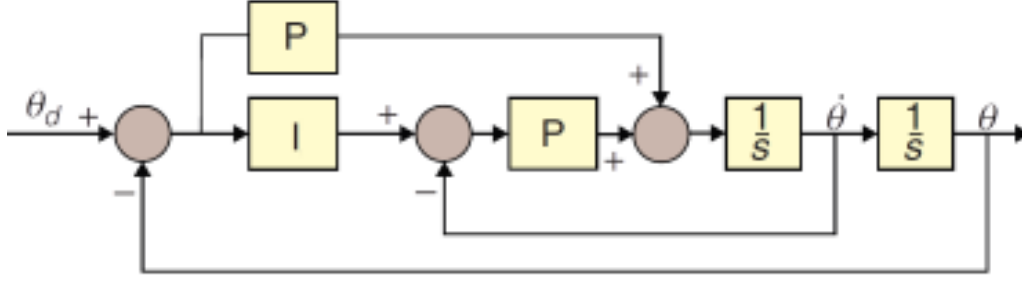
Quadrotor plant dynamics, as mentioned previously, are often simplified; especially when represented with a 3-variable Euler angle set,  $\vec{\mathcal{E}} = [\phi \ \theta \ \psi]^T$ . The coupled gyroscopic and Coriolis responses are both neglected when the angular velocity rate is small,  $\vec{\omega}_b \approx 0$ , and the inertial matrix is diagonal,  $rk(\mathbb{I}_f) = x$  for  $x \in \mathbb{R}^x$ . The consequence of which is the ineffectual deterioration of both the gyroscopic term,  $\vec{\tau}_{gyro} = -\vec{\omega}_b \times \mathbb{I}_b \vec{\omega}_b \approx 0$  and the Coriolis force term,  $\vec{F}_{cor} = -\vec{\omega}_b \times \vec{a}_b \approx 0$  in the bodies dynamics (Chapter:3 for context). Once the coupled cross-product terms are no longer of consequence, the 6 degrees of freedom,  $[x \ y \ z \ \phi \ \theta \ \psi]^T$ , can each be treated as an individual SISO plant controlled with an appropriate technique. Quaternion represented attitude plants cannot easily be decomposed into individual single-input-single-output systems (quaternion dynamics in Section:3.1.3). So a quaternion (combined four variable attitude state vector) is then used,  $Q_b = [q_0 \ \vec{q}]^T$  for the abstracted major loop plant.

Commercial flight controllers (Arducopter [3], Openpilot [47]<sup>10</sup>, BetaFlight [7], etc ...) for custom fabricated UAV platforms all apply their own flavour of structured attitude controllers and state estima-

<sup>8</sup>Quaternion attitude states will replace Euler angles

<sup>9</sup>*The Attitude Control* [82] describes these conventionally different error states

<sup>10</sup>NOTE: OpenPilot's firmware stack is now maintained by LibrePilot



**Figure 1.6:** ArduCopter PI Euler Angle Attitude Control loop

tion algorithms, based on onboard hardware sensor fusion. The article *Build Your Own Quadrotor* [48] summarizes the control structures implemented on a range of common flight controllers. The most popular of which, ArduCopter, implements a feed-forward PI compensation controller (Fig:1.6)<sup>11</sup>. PI, PD and PID controllers are all easy and effective plant independent control solutions for general attitude plants. Table:1.1 collectively lists the common attitude control blocks (not exclusively quadrotors UAVs but MAVs too) and which projects they've been implemented in, after which a critique on the more unique adaptations is given.

Controller Type	Independent	Dependent	Total
PI	[82]	[82]	2
PD	[1, 50]	[23, 57]	4
PID	[10, 12, 69, 73, 82]	[35, 71, 82]	8
Lead	[17, 67]	lead	2
IBC	[51, 75] <sup>12</sup>	[51]	3
ABC	[6, 19, 41, 55]		4
LQR	[12]	LQR	1

**Table 1.1:** A Breakdown of common Attitude Controllers

In a collection of papers, written by Bouabdallah et al ... (2003,2004,2007) arguably the most prolific early quadrotor authors, a range of different control implementations are derived and reviewed. Their last paper (2007) [11] derived and practically tested an Integral Backstepping attitude controller on an OS4 quadrotor. It builds on their research from an earlier paper (2003) [12] wherein an analysis of PID vs LQR attitude controllers in the context of quadrotors is posed. LQR controllers aim to optimize the controller effort (with  $u \in \mathbb{U}$ , controller effort is then  $\|u\|$  or the  $L_2$  norm of the plant input). Although, in theory, solving the associated Ricatti cost function may produce an optimal, stable and efficient control law it needs exact plant matching. In practice, exact plant matching is difficult to achieve for a quadcopter or any aerospace body for that matter. The resultant controller in [12] achieved asymptotic stability but had poor steady state performance due to low confidence of the identified actuator dynamics and poor inertial measurements.

Adaptive Backstepping Control [86](any of the examples in Table:1.1) builds on nominal IBC fundamentals by introducing an additional disturbance state term in the LCF used for the backstepping iteration. The drawback with this form of Backstepping approach is that, from the Lyapunov control theorem, a time derivative for the estimated disturbance (or an *update law*) is needed. Disturbance approximation has been investigated thoroughly but, for a signal without *a priori* information, some heuristic needs to be adopted with the approximation which usually involves some compromise. In one example, [19], the authors implemented a statistical *proj(.)* operator based technique. Which, when used in adaptive control, the projection operator [14], *proj(.)*, ensures a derivative based estimator is bounded for adaptive regression approximation [66].

<sup>11</sup>Image sourced from *Build your own Quadrotor* [48]

Although the control implementation isn't backstepping based, in [90], a sliding mode controller was used to compensate for the disturbances in an Unmanned Submersible Vehicle attitude plant. The underwater current disturbances were approximated using a fuzzy logic system, specifically a *zero-order TSK* fuzzy controller. The TSK system has been proven to act in the same way as an Artificial Neural Network approximator [53]; where the TSK system is more comprehensible than the latter. Statistical analysis and investigation of approximators without *a priori* knowledge of a system are well beyond the scope of this research but are worth mentioning.

### Single/Dual Axis Control & Allocation

The extra actuation introduced with single and dual axis articulation provides room for more control goals to be achieved as the order of actuation increases. Of the few papers published on tilting-axis quadrotors, PD controllers (Nemati et al.[2014] [57] and again in Gasco & Rihani [1, 24]) and PID controllers (Ryll et al.[2012,2013] [73,74]) are the norm for control blocks. For either of these systems there needs to be an allocation rule to distribute a commanded input amongst the actuator set. In [39], Johansen et al.[2012] describes the control allocation problem for a dynamic plant:

*Note in state space Equation:1.3a, it's assumed the plant input<sup>13</sup>,  $\tau$ , has a linear multiplicative relationship with the input response,  $g(x, t, \tau) \iff g(x, t)\tau$ .*

$$\dot{x} = f(x, t) + g(x, t)\tau \quad (1.3a)$$

$$y = l(x, t) \quad (1.3b)$$

With a state  $x \in \mathbb{R}^n$  and  $f(x, t)$  &  $g(x, t)$  being the plant's dynamics and input response respectively. In set point tracking, the output is then *tracking* the state  $y = x$ , and hence  $y \in \mathbb{R}^n$ . In an ideal well posed system the number of actuator inputs equals the number of controllable variable outputs; that being  $\dim(x) = \dim(\tau) \in \mathbb{R}^n$ . In the case where the control input  $\tau \in \mathbb{R}^m$ , if  $m > n$  the problem is then overactuated and a level of abstraction is needed; a virtual control input  $\nu_d$  is designed by a control law  $\nu_d = h(x_e, t)$  to affect dynamics. The goal is to then find a function that maps  $\mathbb{R}^m \rightarrow \mathbb{R}^n$  for an actuator matrix  $u \in \mathbb{U}^m$ . An overactuated plant can be described as:

$$\dot{x} = f(x, t) + g(x, t)\nu_d, \nu_d \in \mathbb{R}^n \quad (1.4a)$$

$$\nu_c = B(x, t, u) \approx B(x, t)u, u \in \mathbb{U}^m, \nu_c \in \mathbb{R}^n \quad (1.4b)$$

$$y = x \quad (1.4c)$$

$B(x, t, u)$  is the effectiveness function which quantifies how the actuator inputs  $u$  relate to the virtual commanded input  $\nu_c$ .  $B(x, t, u)$  can be abstracted to a multiplicative relationship  $B(x, t)u$  if the plant's dynamics permit it, such that;  $B(x, t) \in \mathbb{R}^{n \times m}$ . For generic setpoint tracking the control law will design a desired virtual control input  $\nu_d$ , the allocation rule then has to solve  $u$  for  $\nu_c$  such that a slack variable  $s = \nu_c - \nu_d$  is minimized:

$$\min_{u \in \mathbb{R}^m, s \in \mathbb{R}^n} \|Q_s\| \text{ subject to } B(x, t, u) - h(x_e, t) = \nu_c - \nu_d = s, u \in \mathbb{U} \quad (1.5)$$

Which ensures the commanded input  $\nu_c$  tracks the desired control input  $\nu_d$ ;  $\nu_c \rightarrow \nu_d$  as per some cost function of the slack variable  $Q_s$ . Mostly the L2 norm,  $\|Q_s\|$ , is used. In an overactuated system it then follows that there is a set of possible inputs for each  $\nu_c$ . A unique actuator solution (rather than a family solution set) to Eq:1.5 needs a secondary objective function,  $J(x, t, u)$ . Eq:1.5 then becomes;

$$\min_{u \in \mathbb{R}^m, s \in \mathbb{R}^n} (\|Q_s\| + J(x, t, u)) \text{ subject to } \nu_c - h(x_e, t) = s, u \in \mathbb{U} \quad (1.6)$$

Over-actuation is not something often applied to quadrotors and as a result rather than providing a comprehensive literature review of associated papers here (which are all mostly theoretical derivation), the contextual application and solutions to the above posed problems are expanded later in Section:

<sup>13</sup>Disambiguation:  $\tau$  is not necessarily the torque input.

4.3.1. The only overactuated quadrotor (birotor dual-axis tilting makes the system critically actuated and so requires no allocation) literature which covers allocation of the given actuators is [1, 24], where the authors apply a weighted pseudo inverse (sic Moore Penrose Inverse [45]) allocation rule. A prerequisite for pseudo inversion is a multiplicative (*linear*) control effectiveness relationship for Eq:1.4b.

Segui et al. [2012] applied weighted inversion that relies on some very specific assumptions. For the net torque response, the authors assumed the extra actuators pitch and roll angular rates,  $\dot{\phi}$  and  $\dot{\theta}$  respectively, were proportionally related as follows:

$$\dot{\phi} \approx \frac{\phi}{t_{rise}} \quad (1.7)$$

In which  $t_{rise}$  is the actuators rise time to a set-point. As a result the gyroscopic first order torque  $\tau_{gyro} = -\omega \times \mathbb{I}_f \omega$  and second order inertial torque  $\tau = \mathbb{I} \dot{\omega}$  are then functions of position  $\phi$  or  $\theta$  and not their derivatives. The extent of that consequence is contrasted with the allocation solution in Section:4.3.

## Satellite Attitude Control

Unconstrained attitude set-point tracking for 6-DOF bodies, quaternion based or otherwise, is a topic well covered in the field of satellite attitude control; [38, 42, 84]. The *status quo* for recent research is on non-linear adaptive attitude back-stepping control systems, wherein the adaptive update rule is the novel focus. Often plant uncertainty affects the inertia tensor of a satellite. In [38], the authors Wang Jia, et al. [2010], proposed applying adaptive back-stepping to compensate for steady state (asymmetric) inertial estimation errors. Alternatively, instead of deliberating on costly non-orbital prelaunch inertial measurements, [9] developed an algorithm for estimating the inertia tensor based on single axis controlled perturbations. However that does assume any initial estimates are sufficiently close to true body values such that they will settle and stability can be ensured.

Satellite actuator suites mostly include additional redundant effectors, to ensure fault tolerance and reliability, and hence require control allocation. Often the extra allocators are CMG actuators, driven by DC motors, to produce rotational torques. Fuel burning can only actuate for a certain period of time and so thrusters are scheduled to have a lower priority. Seen in the paper [42]; the authors, Kristiansen et al. [2005], addresses the over-actuation with direct and well-matched inversion before applying quaternion based back-stepping for attitude control. A quadratic pseudo inverse solution to Eq:1.6 is:

$$u = B^\dagger (\tau_a^b - D\omega_{ib}^b) \quad (1.8a)$$

$$B^\dagger = B^T (BB^T)^{-1} \quad (1.8b)$$

Where  $B$  is the control effectiveness matrix and  $B^\dagger$  is such that  $BB^\dagger = \mathbb{I}$ . Specifically  $B^\dagger$  is the general *pseudo* inverse of  $B$  (more on inversions in Sec:4.3). It's assumed there's a multiplicative relationship between the input,  $u \in \mathbb{U}$ , and the input effectiveness matrix in Eq:1.4b. The controller designed actuator torque  $\tau_a^b$  then dictates the input  $u$  as in Eq:1.8a. Much like the over-actuation previously discussed W.R.T quadcopters; the pseudo inversion method of control distribution applies quadratic optimization to the allocation slack cost function, Eq:1.5.



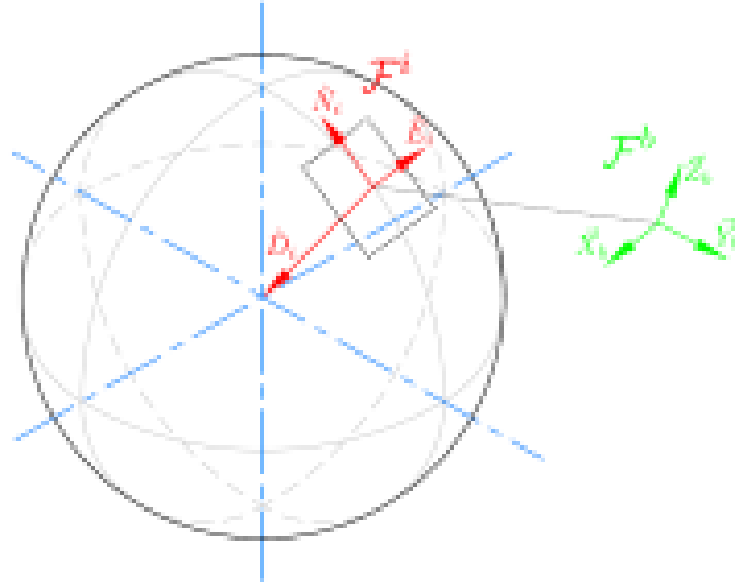
## Chapter 2

# Prototype Design

### 2.1 Conventions Used

The attitude conventions used for the system's dynamic derivations in the following Chapter:3 are first briefly discussed here. Often these aspects are omitted or assumed to be known already. It's important to clearly and unambiguously define a standard set of framing conventions to avoid uncertainty later. Rotation matrices are included but the focus remains on the *contrast* between a rotation and transformation operation. Both [29] and [63] provide an in depth and thorough explanation of rotation matrices and DCM attitude representation if such concepts are unfamiliar to the reader.

#### 2.1.1 Reference Frames Convention



**Figure 2.1:** Inertial and Body Reference Frames

Euler (aerospace) frames are used for principle inertial and body coordinates (Fig:2.1). The inertial frame,  $F^i$ , is aligned such that the  $\vec{X}_i$  axis is in the  $\hat{N}$ orth direction,  $\vec{Y}_i$  is in the  $\hat{E}$ ast direction and  $\vec{Z}_i$  is in the  $\hat{D}$ ownward direction<sup>1</sup>. The body frame,  $F^b$ , then has both  $\vec{X}_b$  and  $\vec{Y}_b$  aligned obliquely between two perpendicular arms of the quadrotor's body and the  $\vec{Z}_b$  axis in the body's normal direction (Fig:2.4). The body frame's axes and their relation to the prototype design are highlighted next in

<sup>1</sup>In orbital sequences this would be toward the Earth's center. Sometimes referred to as the NED convention

Section:2.1.2. Frame superscripts  $i$  and  $b$  represent inertial and body frames respectively whilst vector subscripts imply the reference frame in which the vector's coordinates exists in.

Relative angular displacement between two frames is commonly measured by the three angle Euler set. The Euler angles  $\Upsilon = [\phi \ \theta \ \psi]^T$  represents rotations about the  $\vec{X}, \vec{Y}$  and  $\vec{Z}$  axes respectively. Depending on how the rotation sequence is formulated, those angles can be used to construct rotation matrices which give relation to vectors or can transform coordinates. The generic equation to rotate a vector  $\vec{v}$  about a (normalized) axis  $\hat{n}$  by some angle  $\mu$  is given by<sup>2</sup>:

$$\vec{v}' = (1 - \cos(\mu))(\vec{v} \cdot \hat{n})\hat{n} + \cos(\mu)\vec{v} + \sin(\mu)(\hat{n} \times \vec{v}) \quad (2.1)$$

Which, when  $\hat{n}$  is either  $\vec{X}, \vec{Y}$  or  $\vec{Z}$  axes, can be simplified to produce the fundamental rotation matrices  $\mathbb{R}_x(\phi), \mathbb{R}_y(\theta)$  and  $\mathbb{R}_z(\psi)$ . Multiplication by a rotation matrix  $\mathbb{R}(\cdot)$  applies a left-handed *rotation* operator, the resultant vector still exists in the same reference frame;

$$\vec{v}' = \mathbb{R}_x(\phi)\vec{v} \quad (2.2a)$$

$$\vec{v}', \vec{v} \in \mathcal{F}^1 \quad (2.2b)$$

*No subscripts are used in Eq: 2.2 to indicate reference frame ownership because all vectors are in the same frame*

A *transformation* changes the vectors reference frame. The transformation is a rotation by an angle of the difference between the resulting and principle reference frames. A transformation from frame  $\mathcal{F}^1$  to  $\mathcal{F}^2$ , differing by an angle of  $\phi$  about the  $\vec{X}$  axis is then:

$$\vec{v}_2 = \mathbb{R}_x(-\phi)\vec{v}_1 \quad (2.3a)$$

$$\vec{v}_2 \in \mathcal{F}^2 \text{ and } \vec{v}_1 \in \mathcal{F}^1 \quad (2.3b)$$

The distinction between Eq:2.2 and Eq:2.3 is the sense of the angular operand  $\phi$ , and hence the effect it has on the argument vector. The transformation of a vector from  $\mathcal{F}^i$  to  $\mathcal{F}^b$  is the product of three sequential operations about each axis. Because each subsequent rotation is applied relative to a new intermediate frame, the sequence of axial rotation operations will effect the Euler set. Any consequences of that chosen order is something well documented in *Quaternions and Rotation Sequence*, [43]. In this dissertation the Z-Y-X sequence is used. Hence a transformation of a vector  $\vec{v}$  from the inertial to the body frame is applied by:

$$\mathbb{R}_i^b \triangleq \mathbb{R}_z(\psi)\mathbb{R}_y(\theta)\mathbb{R}_x(\phi) \quad (2.4a)$$

$$\vec{v}_b = \mathbb{R}_i^b(-\psi, -\theta, -\phi)\vec{v}_i \quad (2.4b)$$

$$\Rightarrow \vec{v}_b = \mathbb{R}_z(-\psi)\mathbb{R}_y(-\theta)\mathbb{R}_x(-\phi)\vec{v}_i \quad (2.4c)$$

$$\mathbb{R}_z(-\psi)\mathbb{R}_y(-\theta)\mathbb{R}_x(-\phi) \iff \mathbb{R}_x(\phi)\mathbb{R}_y(\theta)\mathbb{R}_z(\psi) = \mathbb{R}_b^i \quad (2.4d)$$

The relation in Eq:2.4d is an inversion (*transpose*) of the rotation matrix. A rotation matrix's inverse can be used interchangeably to maintain a positive sense of the rotational angle. To ensure clarity throughout this paper's mathematics, a negative angular sense implies a *transformation* to a different reference frame. Where applicable, the order of rotation will indicate the sequence direction and an angular sign differentiates a rotation or transformation operation.

An inherent singularity does exists with such attitude representations. Indeed Quaternions are used for kinematics later in lieu of Euler angles. Euler angular attitude representation is, however, easily understood and well suited to the conventional distinctions made here. Quaternion operations are similarly sequenced in the ZYX order:

$$\mathbb{R}_i^b \iff Q_b^* \otimes (\cdot) \otimes Q_b \quad (2.5a)$$

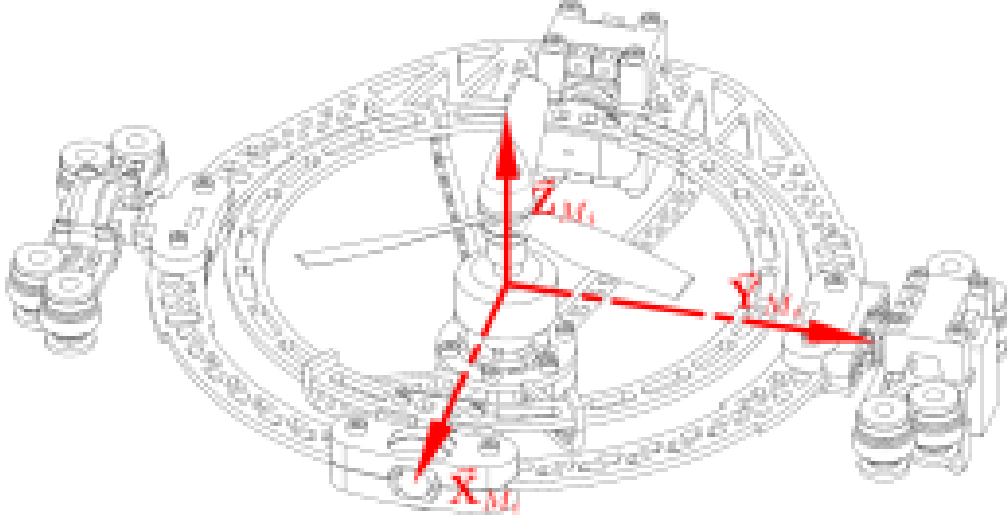
$$Q_b^* \triangleq Q_z^* Q_y^* Q_x^* \text{ and } Q_b \triangleq Q_x Q_y Q_z \quad (2.5b)$$

With  $\otimes$  being the Hamilton product (or quaternion multiplier). Each quaternion,  $Q_i$ , is a unit quaternion about that  $\hat{i}^{th}$  axis. The operator and subsequent quaternion kinematics are defined later in Sec: 3.1.3.

<sup>2</sup>Derived and proven in *Quadrotor Dynamics and Control* [69]

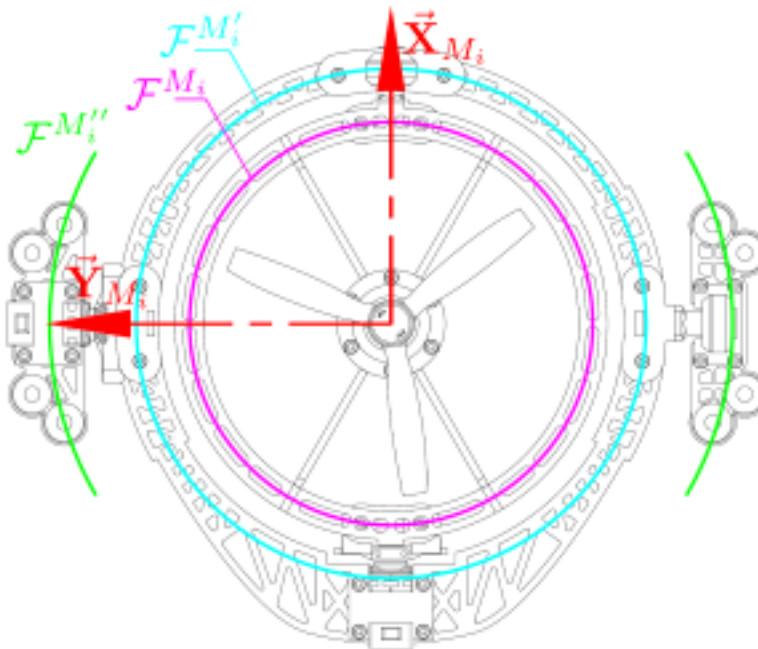
### 2.1.2 Motor Axis Layout

Fundamentally the whole structure, although treated as rigid in the kinematics, consists of multiple bodies able to rotate relative to one another. Each propeller and motor pair is actuated by two servos. If the propeller, attached to the motors' rotor, has a rotational speed  $\omega$  about the  $\vec{Z}$  stator axis, then two servos are aligned with  $\vec{Y}$  and  $\vec{X}$  axes to pitch and roll the propeller away from its principle rotational axis. Each of the four motors has their own reference frame,  $\mathcal{F}^{M_i}$ , aligned as in Fig:2.2.



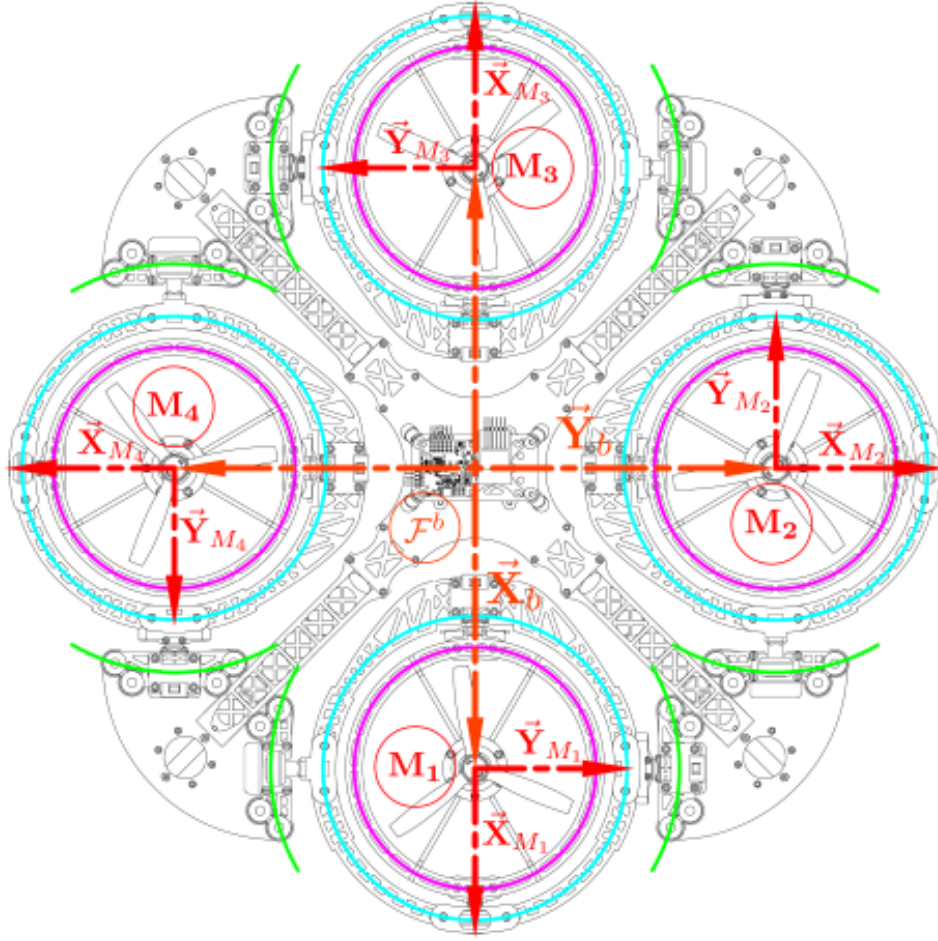
**Figure 2.2:** Aligned Motor Frame Axes

The motor frames, numbered 1 – 4, transform to the body frame first by an angle of  $\lambda_i$  about the  $\vec{X}_{M_i}$  axis. Then by  $\eta_i$  about the  $\vec{Y}_{M'_i}$  axis in an intermediate  $M'_i$  frame. The second servo actuates  $\eta_i$  to produce a second intermediate frame  $M''_i$ , the servo is fixed in the  $M'_i$  frame. Finally there is a relative  $\vec{Z}_{M''_i}$  rotation between  $\mathcal{F}^b$  and  $\mathcal{F}^{M''_i}$ . The layout of all four motor modules are such that the  $\vec{Z}$  axis transformation between the intermediate frame  $\mathcal{F}^{M''_i}$  and  $\mathcal{F}^b$  are all constants; 0, 90°, 180° or 270°. Each modules' state is fully described by  $[\Omega_i, \lambda_i, \eta_i]^T$  for  $i \in [1 : 4]$ .



**Figure 2.3:** Intermediate Motor Frames

The four motor modules are aligned relative to the body's XYZ axes as show in Fig:2.4. Modules 1 and 3 have their X-axes respectively in the positive and negative X direction of the body frame. Similarly Modules 2 and 4 have their X-axes in the positive and negative Y directions of the body frame.



**Figure 2.4:** Body Frame Axes Layout

Not shown in Fig:2.4 is the relative Z axis position with respect to the structure. The Z height of the body's motion centroid such that its origin is co-planar with the four motor modules rotational centres. The centre of motion is not the center of mass, an aspect which is quantified in the following Section:2.2.2.

Transformation relationships from each of the motor frames to the body can be characterized as:

$$\vec{v}_b = \mathbb{R}_z(-\sigma_i)\mathbb{R}_y(-\eta_i)\mathbb{R}_z(-\lambda_i)\vec{v}_{M_i}, \quad \sigma_i \in [0, 90^\circ, 180^\circ, 270^\circ] \quad (2.6a)$$

$$\mathbb{R}_z = \begin{bmatrix} 1 & 0 & 0 \\ 0 & 1 & 0 \\ 0 & 0 & 1 \end{bmatrix}, \begin{bmatrix} 0 & -1 & 0 \\ 1 & 0 & 0 \\ 0 & 0 & 1 \end{bmatrix}, \begin{bmatrix} -1 & 0 & 0 \\ 0 & -1 & 0 \\ 0 & 0 & 1 \end{bmatrix}, \begin{bmatrix} 0 & 1 & 0 \\ -1 & 0 & 0 \\ 0 & 0 & 1 \end{bmatrix} \text{ for } i \in [1, 2, 3, 4] \text{ respectively} \quad (2.6b)$$

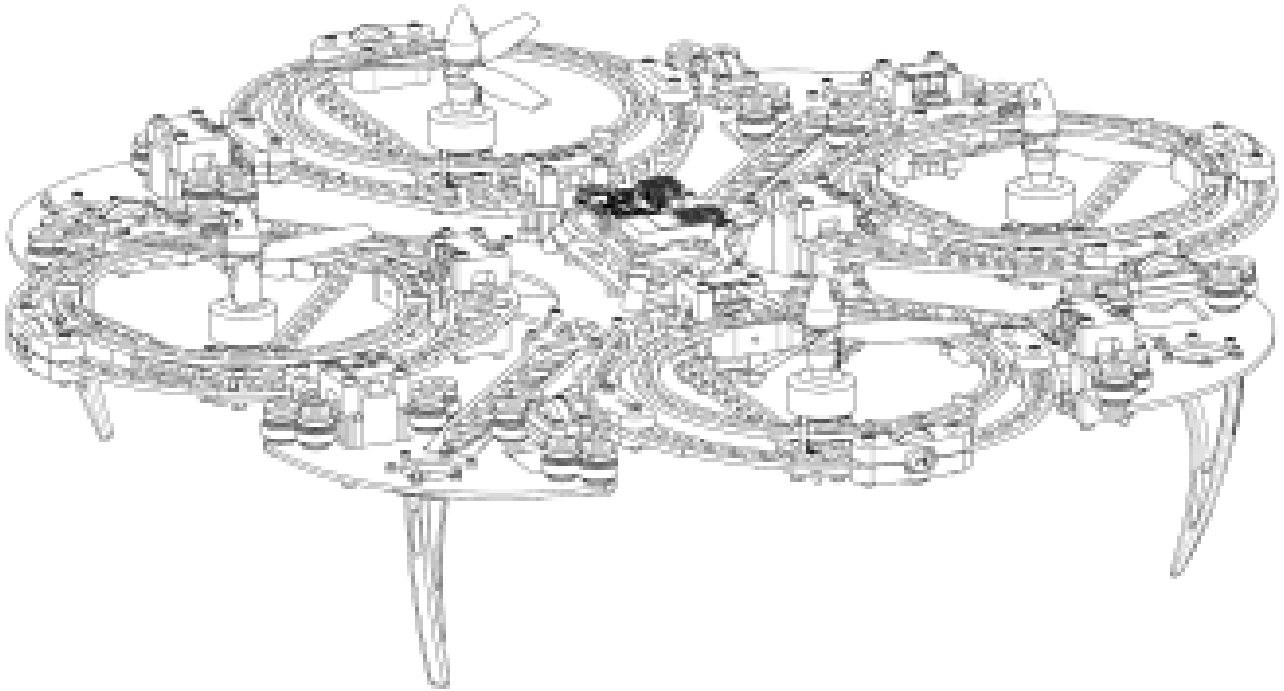
The entire actuator space, including propeller speed  $\Omega_i$  [rps], is then  $(\in \mathbb{R}^{12})^3$ , or rather  $\mathbb{U} \in \mathbb{R}^{12}$ . The actuator input set  $u \in \mathbb{U}$  is then structured as:

$$u_{\in \mathbb{U}} = [\Omega_1 \ \lambda_1 \ \eta_1 \ \dots \ \Omega_4 \ \lambda_4 \ \eta_4]^T \quad (2.7)$$

---

<sup>3</sup>Disambiguation: An omission of axial subscript on the  $\mathbb{R}$  symbol implies a real space of the superscript dimension.

## 2.2 Design



**Figure 2.5:** Isometric layout of the designed prototype

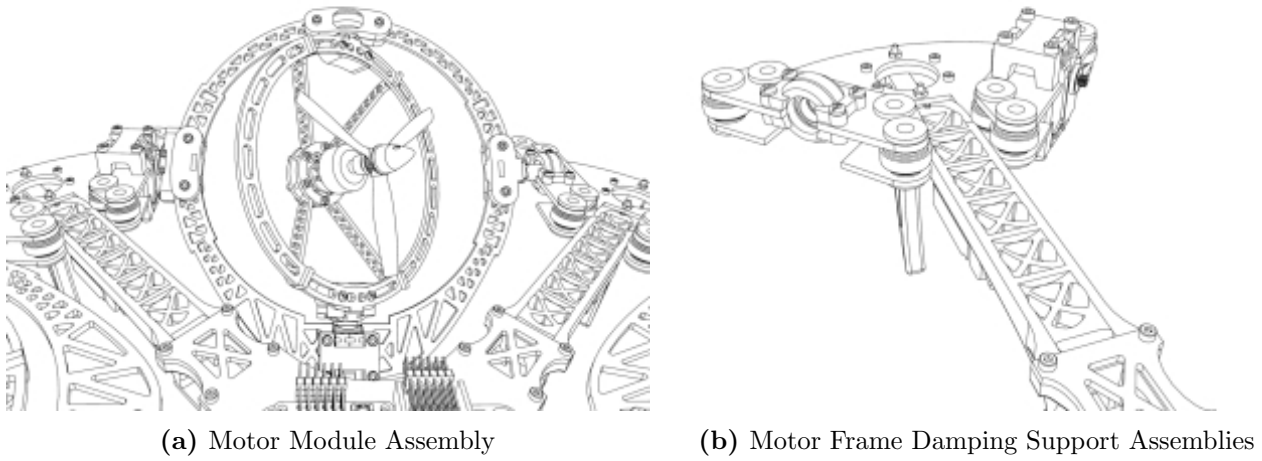
The actual prototype went through a series of different design iterations, all aimed at using as many off-the-shelf RC components as possible whilst attempting to optimize construction costs. A significant factor in the design was the net weight whose upper limit, as mentioned before, is inherently linked to the thrust produced by the motors used. Some of the more important design aspects, like inertias, are discussed here in order to give context to some of the dynamics derived in the next chapter. The actuator suite’s functionality and transfer characteristics are presented here. Finally a brief overview of the electrical systems layout is given with the components associated electrical characteristics listed. A review of the physical prototype realized and control loop implementation is detailed in Chapter:6 along with actual flight test results.

### 2.2.1 Actuation

The novel component of the design is articulation of each motor module, independently redirecting the thrust generated by each lift propeller. Within each module are servos affixed onto sequential rings to pitch and roll the substructure’s axes. The gyroscope-like frame that surrounds each motor/propeller pair accommodates the relative movement. Aligned with each servo is a coaxial support bearing. The coaxial bearing and actuator servos do have a mass disparity that results in an eccentric mass center, producing a gravitational torque arm. Unfortunately, due to weight constraints, counter balance measures cannot be introduced. Consequences from the center of mass variations must either be compensated for (*plant dependent solution*) or exploited in the dynamics (*additional non-linear actuator plants*). The precise effects are quantified numerically next in Section:2.2.2.

Each module is designed such that thrust vector produced coincides with the two rotational axes intersections (Fig:2.6a). There’s no perpendicular displacement of generated thrust vectors relative to the body’s X-Y-Z origin<sup>4</sup>. It’s more prudential to ensure intersection of the thrust vector with the rotational center than to balance the masses undergoing rotation. A thrust varying torque is harder

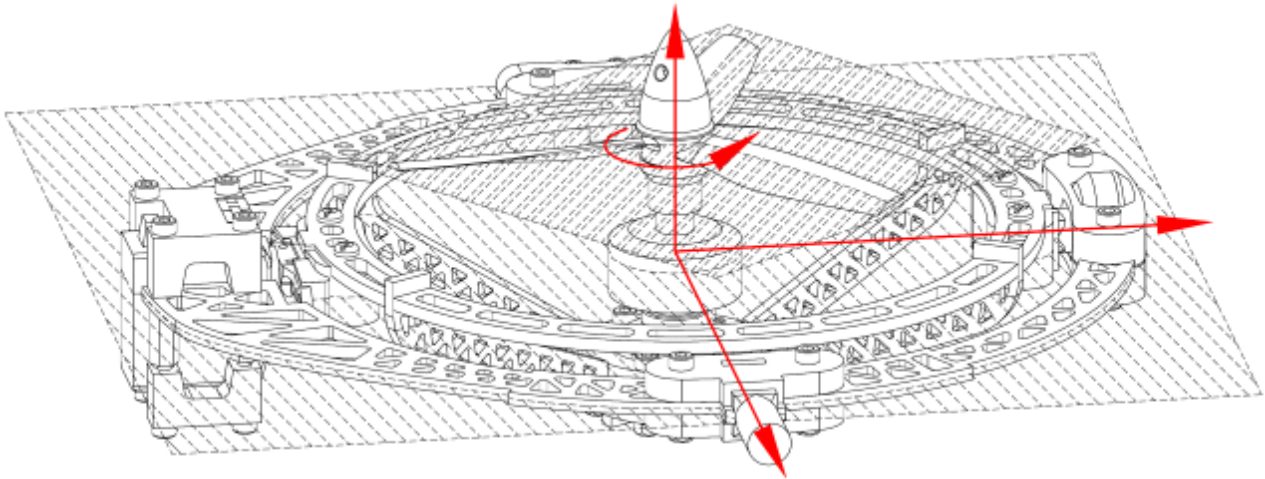
<sup>4</sup>Although the center of gravity does have a time varying position dependent on the 8 servos positions



**Figure 2.6:** Motor Assembly

to compensate for than a gravitational torque given the complexity with modelling a propeller's aerodynamic thrust (Section:3.3.1).

The primary frame has silicon damping balls between brackets which attach to the motor gyroscope assembly (Fig:2.6b). For damping to be effective there has to be roughly equatable relative masses between the two damped bodies. A smaller damping assembly in the center of the frame houses all the electronics and power distribution circuitry. All the mounting brackets which affix the motor modules are 3D printed from CAD models using an Ultimaker V2+ [85]. There is a complete bill of materials for all parts used, including working drawings for each 3D printed bracket and the laser cut frame(s), in Appendix:B.

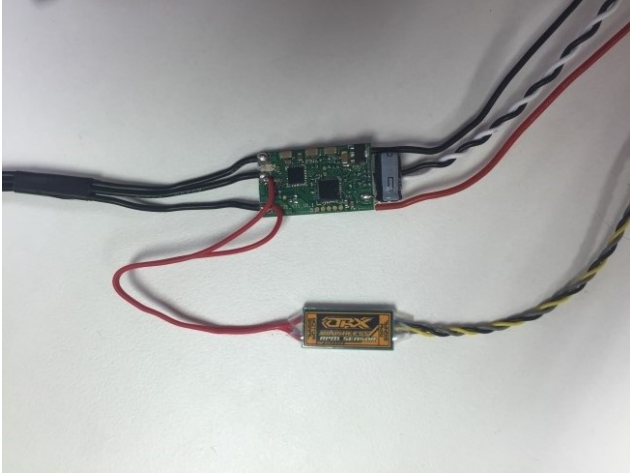


**Figure 2.7:** Difference between propeller and motor planes

The propellers rotational plane is not exactly aligned with the plane made by the  $\vec{X}_{M_i}$  and  $\vec{Y}_{M_i}$  rotational servo axes (Fig:2.7). The offset is approximately 28.2 mm and must be considered when evaluating pitch/roll gyroscopic torque responses later in Section:3.2.1. The propellers are 6 inch ( $6 \times 4$ ) 3-Blade plastic Gemfam propellers, powered Turnigy DST-700KV Outrunner Brushless DC motors. The thrust produced as a function of angular velocity (in RPS) for the propellers is derived in Section:3.3.1. The BLDC motors are controlled with Hobbywing XRotor 15A ESC modules with an inline Orange RPM Sensor. The transfer function for the combined unit is presented subsequently in Section:2.3.1. Power for the quadrotor is supplied not from a battery bank but from a power



tether. Tethered power will ensure consistent flight time and reduce the concern of payload strain on the available lift actuation. Power lines to both the BLDC motors and servos are both supplied conventionally, however an ideal construction would see slip-rings for each module's supply. Power transmission lines are affixed such that they don't impede rotation.



(a) BLDC ESC & RPM Sensor Assembly



(b) Turnigy DST-700KV BLDC Motor

Metal gear Corona DS-339MG digital servos are used for the two axes of rotation (Fig:2.9). Each servo has a range of  $180^\circ$ , positioned such that a zero<sup>th</sup> offset aligns the motor modules adjacent to the body frame and has a  $\pm 90^\circ$  range. A digital servo updates at 330 Hz, faster than a 50 Hz analogue servo equivalent (Table:2.1). This means the otherwise 20ms zero-order analogue sampling becomes a less significant 3.30ms zero-order holding time. Both the  $\vec{X}_{M_i}$  and  $\vec{Y}_{M_i}$  axis servos will be rotating a large loading mass and so their *open loop* plant dynamics are determined empirically in Section:2.3.1 using test data included in Appendix:C.

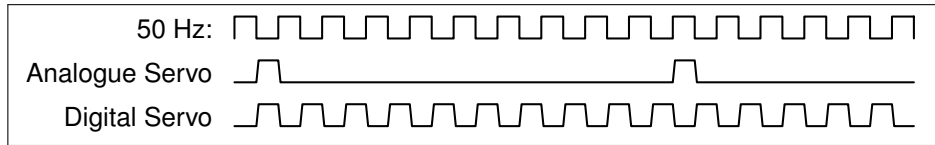


Table 2.1: Analogue & Digital Timing Signals

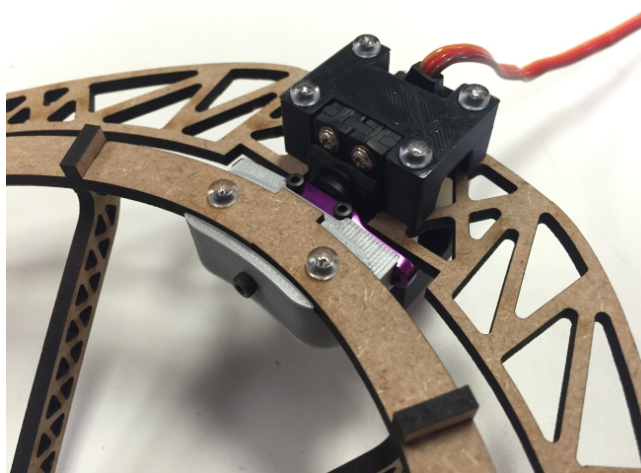


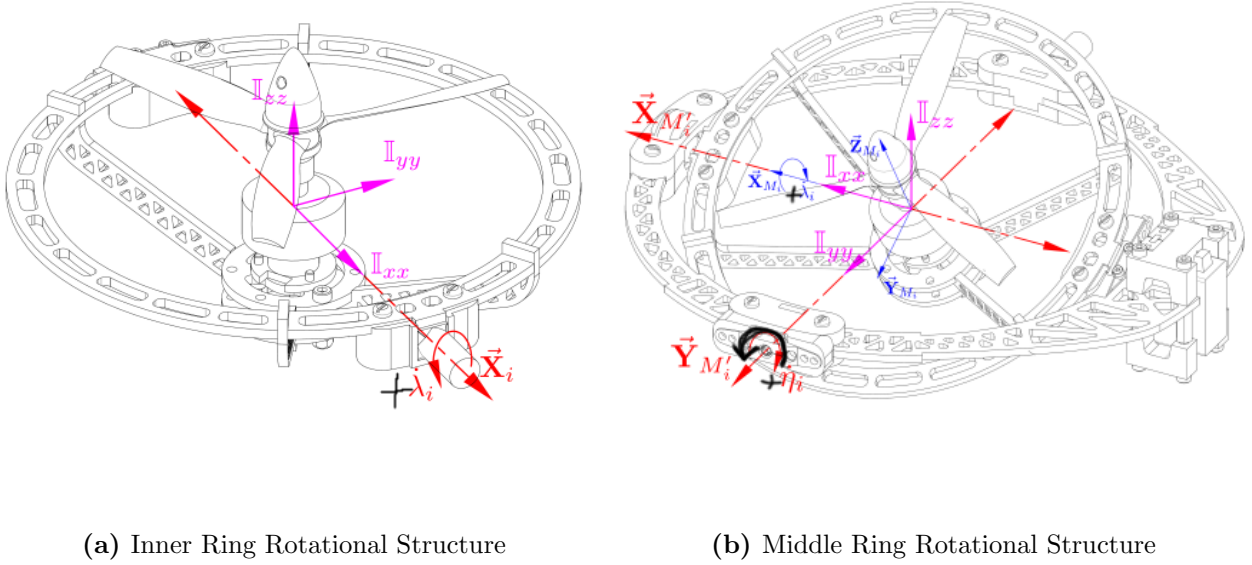
Figure 2.9: Corona Servo Bracket

### 2.2.2 Inertial Matrices & Mass

Although inertias are presented here rounded to either 2 or 0 decimal places, full floating point numbers are used in simulation and prototype software. Un-rounded inertias are included in Appendix:D. Similarly rotation matrices produce a more cumbersome results for Eq:2.92.122.14, which are susceptible to singularities. Quaternion operators are used in practice.

#### Inertias

An undesirable side effect of the rigid body rotations the structure undergoes are the inertial responses produced from such movements. Given Newton's Second Law of Rotational Motion<sup>†</sup>, the applied rotations are going to produce an equal but opposite reaction onto the principle inducing frame. Similarly a gyroscopic cross product from rotational velocities is also present. Such first and second order effects are often neglected given that angular rates are mostly small enough to approximate as zero,  $\vec{\omega}_b \approx \vec{0}$ . A dynamic set-point (non-zero) attitude tracking plant is, however, going to produce sizable time varying body angular velocities and accelerations. Unlike a traditionally actuated quadrotor, such effects have to be accounted for.



**Figure 2.10:** Inertial Measurement References

The manifestation of the aforementioned torques are explored in thorough detail in Section:3.2. Those effects are both dependent on the rotational body's inertial tensor<sup>5</sup> about each respective rotational axis. The magnitude of those inertias are obviously a by-product of the structure's design. Starting with the innermost assembly, in each Motor Frame  $\mathcal{F}^{M_i}$ , the inside ring structure is a 99g assembly (all components incorporated). The rotational center *roughly* coincides with the center its of mass ( $C.M = [-1.40 \ -0.04 \ -1.94]^T$  [mm] relative to its rotational center). The inner ring being rotated by  $\lambda_i^\circ$  about the  $\vec{X}_{M_i}$  axis then has an inertial matrix (centered and aligned with axes as in

<sup>5</sup>All inertias are assumed asymmetrical and calculated in Solidworks with overridden masses to match physical prototype, all the measurements are included in Appendix:B



Fig:2.10a):

$$\mathbb{I}_{M_i} = \begin{bmatrix} 588.84 & -0.28 & 0.25 \\ -0.28 & 1966.60 & 0.90 \\ 0.25 & 0.90 & 2141.78 \end{bmatrix} [g.cm^2] \quad (2.8a)$$

$$\approx \text{diag}(588, 1966, 2141) \times 10^{-7} [kg.m^2] \quad (2.8b)$$

The effect of rapidly spinning propellers on the inertia in Eq:2.8a is approximated well by a solid disc, hence the inner ring's off-diagonal inertial products are regarded as negligible. The moment of inertia about that  $\vec{X}_{M_i}$  axis, pertinent to a  $\lambda_i$  rotation, is then  $\mathbb{I}_\lambda = 588.84 \times 10^{-7} [kg.m^2]$ .

The first  $\lambda_i$  actuating servo and bearing supports are affixed to the intermediate middle ring assembly (Fig:2.10b). The middle ring frame,  $\mathcal{F}_{M_i}'$ , is a 102g structure, excluding the inner most ring. Collectively the mass for both the inner and middle rings structures is  $m_{module} = 201g$ . That middle ring is rotated by  $\eta_i^\circ$  about its  $\vec{Y}_{M_i}$  axis. The compound body's inertia about that axis of rotation,  $\vec{Y}_{M_i}$ , is a combination of both the middle ring's inertia and the inner ring's. The latter contribution being a function of the *rotation* (not transformation) angle  $\lambda_i^\circ$  which, from the conservation of angular momentum theory [64]<sup>6</sup>, is:

$$\text{If } \mathbb{I}_{middle} = \begin{bmatrix} 3024.30 & 0.03 & 406.84 \\ 0.03 & 8791.16 & 0.01 \\ 406.87 & 0.01 & 11579.85 \end{bmatrix} [g.cm^2] \quad (2.9a)$$

$$\mathbb{I}_{M_i}' = \mathbb{I}_{middle} + \mathbb{R}_X(\lambda_i)(\mathbb{I}_{inner})\mathbb{R}_X^{-1}(\lambda_i) \quad (2.9b)$$

$$\mathbb{I}_{M_i}'(\lambda) = \mathbb{I}_{const} + \mathbb{I}_{M_i}(\lambda) \quad (2.9c)$$

$$\approx \begin{bmatrix} 3609 & 0 & 407 \\ 0 & 10842 & 0 \\ 407 & 0 & 13630 \end{bmatrix} + \begin{bmatrix} 0 & 0 & 0 \\ 0 & -88c_{2\lambda} & 2c_{\lambda}^2 - 91s_{2\lambda} \\ 0 & 2c_{\lambda}^2 - 91s_{2\lambda} & 88c_{2\lambda} \end{bmatrix} \times 10^{-7} [kg.m^2] \quad (2.9d)$$

With  $\mathbb{I}_{inner} = \mathbb{I}_{M_i}$  being the inertia from Eq:2.8a, transformed by a rotation  $\mathbb{R}_x(\lambda_i)$ . The net inertia being a function of rotation angle,  $\lambda_i$ , and a constant inertia (Eq:2.9c) is then simplified<sup>7</sup> to Eq:2.9d. It's important to note the non-zero product of inertia,  $\mathbb{I}_{yz}$ , which is going to result in a  $\tau_z$  response. The inertia then encountered by an  $\eta_i$  rotation is:

$$\mathbb{I}_\eta(\lambda) \approx [0, 10842 - 88c_{2\lambda}, 2c_{\lambda}^2 - 91s_{2\lambda}]^T \times 10^{-7} [kg.m^2] \quad (2.10)$$

Variable inertias dependent on state input variables are the first of many non-trivial aspects unique to this aircraft's design. The resultant control solutions are thus decidedly plant dependent in their formulation. Secondly, the center of mass for the motor module's compound assembly isn't coincidental with either rotational axes intersection. As a result the effective center of mass for the entire structure is going to be time varying, dependent on the angular rotational position of each motor module.

The second  $\eta_i$  rotating servo joins the complete motor module (both the inner and middle ring assemblies) to the body structure. The inertial volume of the servo and bearing supports contribute then to the body's inertia, whose value excludes any of the four motor modules. Consisting of servo and bearing damping brackets, the "damping" assembly collectively weighs 84g and suspends the motor modules from the body frame with a set of silicon damping balls. The body assembly's center of mass (Fig:2.11) coincides with the XY directional axes and lies  $\Delta Z = -14.27 \text{ mm}$  below the Body Frame's origin of motion,  $\vec{O} \in \mathcal{F}^b$ .

*Note: the origin which all motion is calculated with respect to is co-planar to the motor module's rotational centers, not the net center of mass.*

<sup>6</sup> $\mathbb{R}_x$  is a full rank and square, so an inverse  $\mathbb{R}_x^{-1}$  always exists

<sup>7</sup>Eq:2.9d is rounded to no decimal places, seeing that its units are already  $\times 10^{-7}$

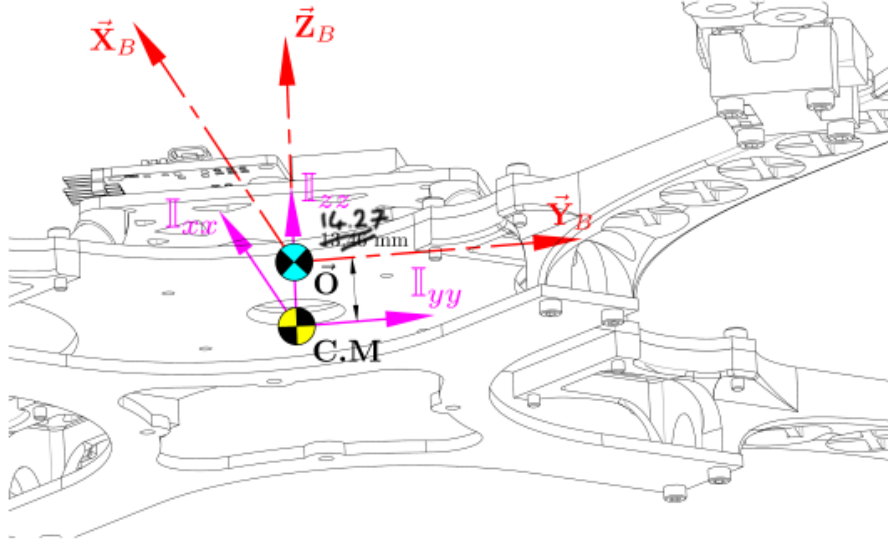


Figure 2.11: Body Frame Center of Mass

The body's weight, including all four damping assemblies, totals to 814.7 g. The body's net inertia (*sans* motor modules)  $\mathbb{I}_{body}$ , about its center of mass is:

$$\mathbb{I}_{body} = \begin{bmatrix} 182018.63 & -0.44 & -80.30 \\ -0.44 & 181896.17 & -17.75 \\ -80.30 & -17.75 & 360077.58 \end{bmatrix} [g.cm^2] \text{ or } \times 10^{-7} [kg.m^2] \quad (2.11a)$$

Using the Parallel Axis theorem<sup>†</sup>, that same net body inertia about the body frame's origin,  $\vec{O}_b$ , is:

$$\mathbb{I}_{body}' = \mathbb{I}_{body} + m(\vec{d} \cdot \vec{d} + \vec{d} \otimes \vec{d}^T) \approx \mathbb{I}_{body} + md^2 \quad (2.11b)$$

Here  $\otimes$  represents the Hamilton product of two  $3 \times 3$  matrices, it's used again later in Chapter:3 to indicate the quaternion multiplication operator.

$$\mathbb{I}_{body}' = \begin{bmatrix} 183677.51 & -0.42 & -4.45 \\ -0.42 & 183555.03 & -10.41 \\ -4.45 & -10.41 & 360077.62 \end{bmatrix} \times 10^{-7} [kg.m^2] \quad (2.11c)$$

Net inertia for the compound assembly,  $\mathbb{I}_b$ <sup>8</sup>, about that origin  $\vec{O}_b$  is a combination of all the relative attached bodies. That being; the four motor modules, transformed and then translated to the center of motion, and the body structure itself. That transformation is analogous to that of Eq: 2.6. Reiterating that the the origin is co-planar to the modules center of rotation, each motor modules inertia,  $\mathbb{I}_{M_i}'$ <sup>9</sup>, is further rotated by  $\eta_i^\circ$  about  $\vec{Y}_{M_i}$  and finally an orthogonal  $\vec{Z}$  rotation onto  $\mathcal{F}^b$ . Still measured with respect to their individual centers,  $\vec{M}_i$ , but re-oriented to align with  $\|\vec{O}_b$ . Contribution of each motor module's inertia, with  $\mathbb{R}_Z$  being the same as Eq:2.6b, is then:

$$\mathbb{I}_{i^{th}motor} = \mathbb{R}_Z(\sigma_i) \mathbb{R}_Y(\eta_i) (\mathbb{I}_{M_i}') \mathbb{R}_Y^{-1}(\eta_i) \mathbb{R}_Z^{-1}(\sigma_i) \quad (2.12a)$$

Expanding to Inner and Middle Ring components:

$$= \mathbb{R}_Z \mathbb{R}_Y(\eta) (\mathbb{I}_{middle}) \mathbb{R}_Y^{-1}(\eta) \mathbb{R}_Z^{-1} + \mathbb{R}_Z \mathbb{R}_Y(\eta) \mathbb{R}_X(\lambda) (\mathbb{I}_{inner}) \mathbb{R}_X^{-1}(\lambda) \mathbb{R}_Y^{-1}(\eta) \mathbb{R}_Z^{-1} \quad (2.12b)$$

$$\text{With axes } \vec{X} \in \mathcal{F}^{M_i}, \vec{Y} \in \mathcal{F}^{M_i'}, \vec{Z} \in \mathcal{F}^{M_i''} \quad (2.12c)$$

*It's at this stage that, despite simplifications, the symbolic inertial equation becomes overly cumbersome to include with numeric values... For the sake of brevity, exact calculated inertia values for the input dependent plant are omitted.*

<sup>8</sup>Disambiguation:  $\mathbb{I}_b$  is *net* body frame's inertia, different from  $\mathbb{I}_{body}$  which is the inertia for *just* the body structure

<sup>9</sup>As defined in Eq:2.9d

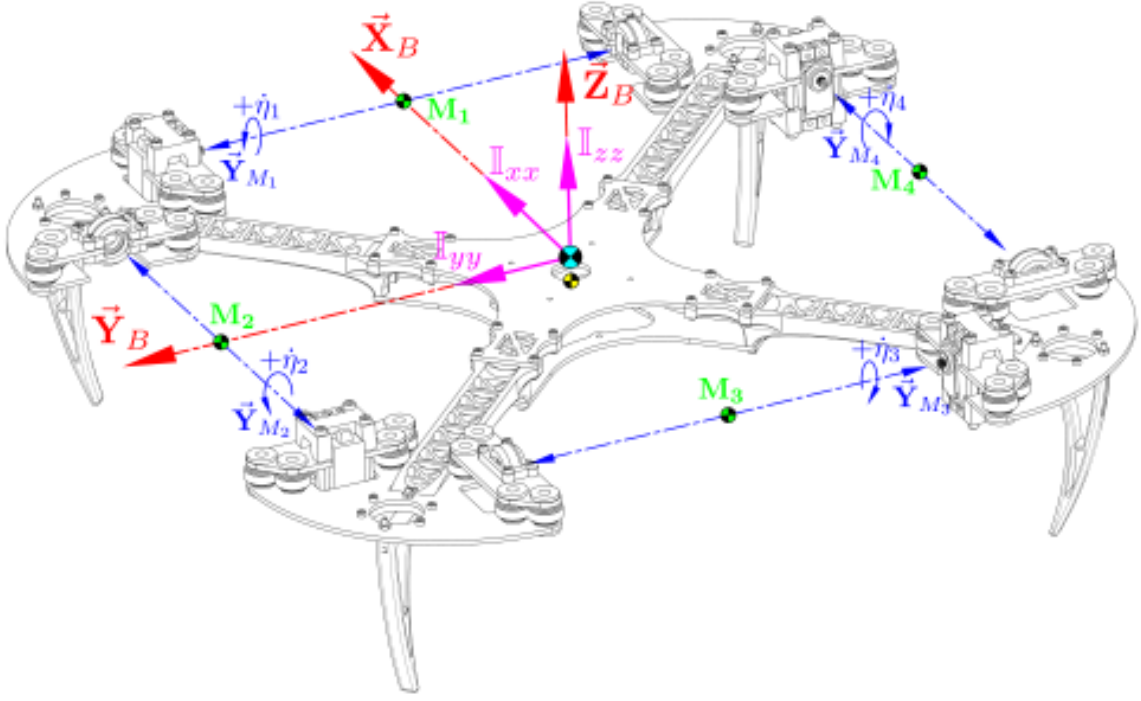


Figure 2.12: Inertial Center &amp; Mass Center

Each module's rotational center is spaced equally relative to  $\vec{O}_b$  with a parallel axis arm  $\vec{L}_{arm} = [195.16 \ 0 \ 0]^T$  [mm] (Fig:2.12). The net inertial equation about  $\vec{O}_b$ , dependent on the actuator suite  $\mathbb{U}$  positions, can be calculated as:

$$\mathbb{I}_b(u) = \mathbb{I}_{body} + \sum_{i=1}^4 \mathbb{M}_i \quad [kg.m^2] \quad (2.13a)$$

$$\mathbb{M}_i = \mathbb{I}_{i^{th}motor} + m_{module}(\vec{L} \cdot \vec{L} - \vec{L} \otimes \vec{L}) \quad (2.13b)$$

Although Eq:2.13 does indeed produce the net body's inertia, the transformations to calculate  $\mathbb{M}_i$  are compounded. Inertias are first translated to the center of rotation from their center of masses and then finally to the body frame's origin. Subsequent transformations are successively going to deteriorate the floating point precision of the resultant inertial tensor. Transforming inertial tensors about each sub-body's center of mass directly to the body frame origin will improve the reliability of the produced inertial equations. It is perhaps more intuitive to consider each sub-body's contribution individually, despite having been derived as combined inertial systems previously.

$$\mathbb{I}_b(u) = \mathbb{I}_{body} + \sum_{i=1}^4 \mathbb{M}_{inner} + \sum_{i=1}^4 \mathbb{M}_{middle} \quad (2.14)$$

The relative movement pertinent to Eq:2.8 and Eq:2.9 are conceptually separated from that affecting Eq:2.13. For each inner ring, W.R.T its center of mass measured relative to its center of rotation, different from Eq:2.8a, the inner ring's inertia is calculated as;

$$m_{inner} = 99 \quad [g] \quad (2.15a)$$

$$\mathbb{I}_{inner}^{C.M} = \begin{bmatrix} 585.11 & -0.34 & -2.44 \\ -0.34 & 1960.93 & 0.81 \\ -2.44 & 0.81 & 2139.84 \end{bmatrix} \quad [g.cm^2] \quad (2.15b)$$

$$C.M_{inner} = [1.400 \ -0.043 \ -1.942]^T \quad [mm] \quad (2.15c)$$

$$C.M_{inner}' = \mathbb{R}_Z \mathbb{R}_Y \mathbb{R}_X (C.M_{inner}) \quad (2.15d)$$

$$\mathbb{I}_{inner} = \mathbb{R}_Z \mathbb{R}_Y (\eta) \mathbb{R}_X (\lambda) (\mathbb{I}_{inner}) \mathbb{R}_X^{-1} (\lambda) \mathbb{R}_Y^{-1} (\eta) \mathbb{R}_Z^{-1} \quad (2.15e)$$

$$\Delta L = \vec{L}_{arm} - C.M_{inner}' \quad (2.15f)$$

$$\mathbb{M}_{inner} = \mathbb{I}_{inner} = \mathbb{I}_{inner} + m_{inner} ((\Delta L \cdot \Delta L) \mathbb{I}_{3 \times 3} - \Delta L \otimes \Delta L) \quad (2.15g)$$

Similarly for each middle ring:

$$m_{middle} = 102 \text{ [g]} \quad (2.16a)$$

$$\mathbb{I}_{middle} = \begin{bmatrix} 2996.57 & 179.32 & 232.71 \\ 179.32 & 6524.84 & 13.87 \\ 232.71 & 13.87 & 9312.733 \end{bmatrix} \text{ [g.cm}^2\text{]} \quad (2.16b)$$

$$C.M_{middle} = [47.00 \quad 3.74 \quad -3.63]^T \text{ [mm]} \quad (2.16c)$$

$$C.M_{middle}' = \mathbb{R}_Z \mathbb{R}_Y (C.M_{middle}) \quad (2.16d)$$

$$\mathbb{I}_{middle} = \mathbb{R}_Z \mathbb{R}_Y (\eta) (\mathbb{I}_{middle}) \mathbb{R}_Y^{-1} (\eta) \mathbb{R}_Z^{-1} \quad (2.16e)$$

$$\Delta L = \vec{L}_{arm} - C.M_{middle}' \quad (2.16f)$$

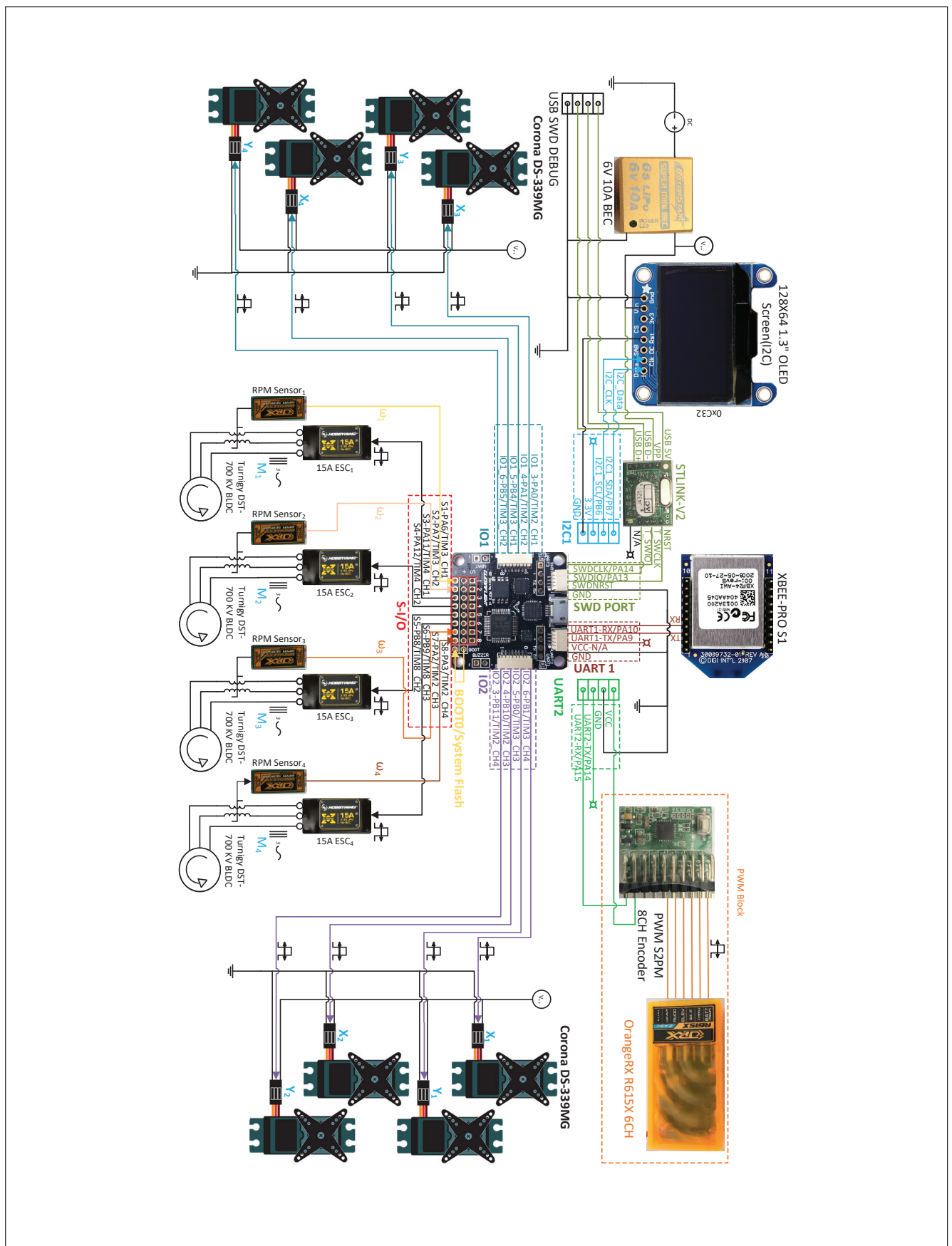
$$\mathbb{M}_{middle} = \mathbb{I}_{middle} = \mathbb{I}_{middle} + m_{middle} ((\Delta L \cdot \Delta L) \mathbb{I}_{3 \times 3} - \Delta L \otimes \Delta L) \quad (2.16g)$$

Unless otherwise specified; any inertia  $\mathbb{I}_b$ , irrespective of arguments, will refer to an instantaneous calculated solution to Eq:2.14 given a particular  $u \in \mathbb{U}$ . The purpose of the derivations Eq:2.15 & Eq:2.16 is twofold; highlighting both the inertial contributions and the variable center of masses for each sub-body. Seeing that the origin of the motion frame  $\mathcal{F}^b$  and the net body's center of mass aren't coincidental, it's important to quantify the equation for the varying center of mass. If, for a collection of  $n$  bodies, with each body's center  $\vec{X}_i$  and a mass  $m_i$ , the net center of mass is:

$$C.M = \frac{\sum_{i=1}^n m_i \cdot \vec{X}_i}{\sum_{i=1}^n m_i} \quad (2.17a)$$

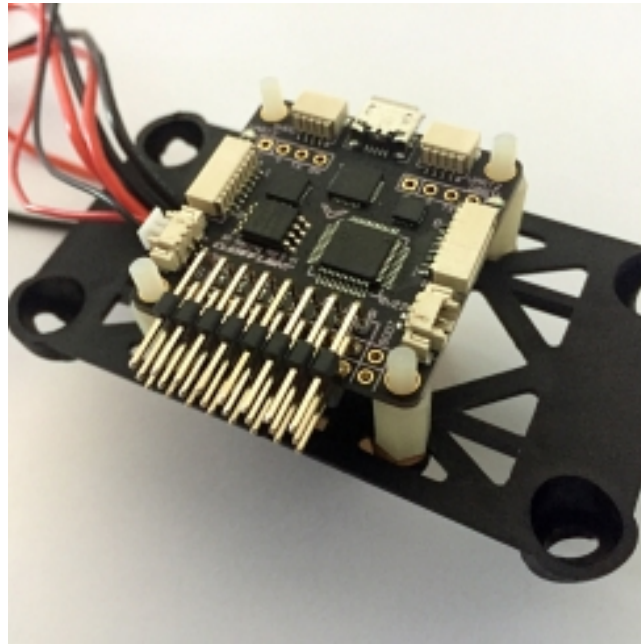
So then, with  $\vec{X}_{inner}$  &  $\vec{X}_{middle}$  being defined in Eq:2.15d & Eq:2.16d respectively, the body has a center of mass<sup>†</sup>:

$$= \frac{m_{body} \cdot \vec{X}_{body} + \sum m_{inner} \cdot \vec{X}_{inner} + \sum m_{middle} \cdot \vec{X}_{middle}}{m_{body} + \sum m_{inner} + \sum m_{middle}} \quad (2.17b)$$



**Figure 2.13:** Hardware Schematic Diagram

An abstracted hardware diagram for the (electronic) system layout is shown in Fig:2.3. It's an illustration for the connection of different electronic peripherals used to aid the on-board control system. The structure of the autopilot system and control loops are addressed in a later Chapter:6. This description aims to provide a brief overview of the specific modules used, their purpose and how they're interfaced. No code structure or control loops are considered yet...



**Figure 2.14:** SPRacing F3 Deluxe Flight Controller

The entire system is constructed around an ARM STM32F303 [79] based  $\mu$ controller. The micro-processor board is a commercial flight control board, specifically an SPRacing F3 Deluxe [16]<sup>10</sup>, which has had its bootloader removed and custom firmware, unique to this project, burnt to it. That software is later described in 6; the I/O for all the peripherals are detailed here however. The on-board flight-controller is an I2C MPU-6050 [36] 6-axis gyroscope & accelerometer with a connected HMC5883 [22] magnetometer compass, an SPI MS5611 [77] barometer and similarly 64 Mb of SPI flash memory. The connections of which are listed in App:B.2.

*The combination of above sensors fused for state estimation and their associated algorithms are dealt with in Section:5.3 in Chapter:5.*



**Figure 2.15:** S.BUS Data Stream

Two wireless communication peripherals are used. First the system relays full state information, for a complete 6-DOF autopilot system, from a ground control station using 2.4 GHz XBEE S1 module(s) [37], USART connected. Secondly, an augmented pilot control input system, fail safe and secondary to autopilot, is transmitted through 6 Channel 2.4 GHz R/F comms. The 6 CH received signals, otherwise permeated as six individual 20 KHz PWM signals via an OrangeRx R615x [60] receiver, are encoded to a single line S.BUS data stream. The S.BUS encoder [33] implements a USART derivative communications standard, Fig:2.15 shows the sampled data stream used to ascertain the following parameters:

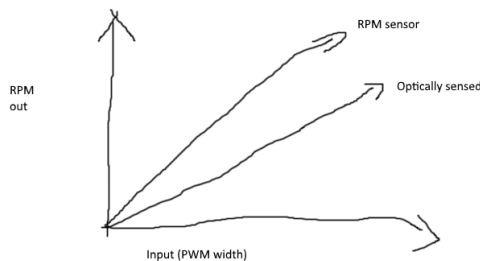
<sup>10</sup>CleanFlight opensource software is regularly used for the F3 but hardware specifications are not openly available. The reverse engineered electrical schematic for the board is included in Appendix:B.2



- 8-Bit data bytes
- 25 Bytes per transmissions
- Bytes are:
  - MSB First
  - 1 start bit
  - 2 stop bits
  - Even parity bit
  - Inverted
  - 100000 baud (bps)
- 14 ms idle time between transmissions
- Up to 16 channels encoded
- Each channel is 11 bits of data
- Channel data is little endian prioritized

The received information of the transmitted 6 channels are filtered through an Infinite-Impulse Response filter. The filters frequency response is as follows:  $y_n = y_{n-1}$ . Any referenced signals received are all post filtered data. Filtering for state estimates is separately performed on the Ground Control Station computer.

Each of the eight digital servo actuators are driven individually from 330 Hz PWM timer output compare channels, pulses ranging from 1ms - 2ms linearly control the rotary position. The exact transfer function is empirically determined next in Section:2.3.1. Four 15A brushless DC speed controllers (ESCs) are each driven from a 20 Hz PWM timer channel output, similarly with 1ms - 2ms pulse widths. There are a total of 12 PWM output compare signals drawn from the  $\mu$ controller. Servos are powered by a regulated 6V DC 10A power supply [32] whilst the ESCs switch unregulated 15.1V DC from an externally tethered power supply. The DC supply could potentially be drawn from an on-board battery bank but that would add significant weight to an already heavy platform.



(a) RPM sensor gain



(b) ST-Link V-2 Debugger

**Figure 2.16**

There's no integrated feedback for instantaneous RPM values from the Electronic Speed Controllers. Using discrete OrangeRX BLDC RPM sensors [31], measuring the phase of back Emf induced across two of the three motor phases, the exact RPM can be ascertained. The signal produced by the

RPM sensors varies the period, proportional to the rotational speed of the motor, of a square wave with a constant 50% duty cycle. The RPM sensor's output signal is calibrated to a *rate* gain, the linear relationship is shown in Fig:2.16a. Knowing exact RPM rates means the subsequent thrust and aerodynamic torques for the control plant inputs can be calculated.

Any STM32  $\mu$ controller is programmed through a dedicated debugging device. The ST-Link V2 [78] is the current proprietary device which, itself, is a specially programmed STM32F10 chip (Fig:2.16b). The chip connects to the dedicated Serial Wire Debugging ports of the target STM (*SWD-CLK*, *SWD-IO* & *SWD-NRST*) and is interfaced via regular USB+ and USB- data lines.

### 2.3.1 Actuator Transfer Functions

Thaar be transfer functions here...



## Chapter 3

# Kinematics & Dynamics

The body's dynamics are first solved as rigid, with appropriate equations derived for generic 6-DOF motion. There after, non-linear aerodynamic and inertial effects, unique to multi-body relative rotations, are presented and included in the plant's model. Finally a consolidated, quaternion based plant model is presented which is used for the later control plant development next in Chapter:4.

### 3.1 Rigid Body Dynamics

#### 3.1.1 Lagrange Derivation

Fundamentally any body, rigid or otherwise, can undergo two kinds of movements, namely rotational and translation motions. Often a Lagrangian [68, 81] approach for combined angular and translational movements is used to derive the differential equations of motion for each degree of freedom. The Lagrangian principle ensures that translational, rotational and potential energies are conserved throughout the system's trajectory progression. When combined with Euler-Rotational equations, the Euler-Lagrangian [83] formulation fully defines the aerospace 6-DOF equation set.

Lagrangian formulation is regarded as especially useful in non-cartesian (*spherical etc. . .*) co-ordinate frames and multi-body systems. With that being said, a cartesian co-ordinate system was already defined in Section:2.1.2, rigid body dynamics in a cartesian co-ordinate frame do lend themselves to Newtonian mechanics. The Newtonain-Euler or Euler-Lagrange formulations produce the same result. The Lagrangian operator,  $\mathcal{L}$ , is a term made up of the difference between kinetic and potential energies,  $T$  and  $U$  respectively, for a path  $\mathbf{r}(t)$  such that;

$$\mathcal{L}(\mathbf{r}, \dot{\mathbf{r}}, t) = T(\mathbf{r}, \dot{\mathbf{r}}) - U(\mathbf{r}, \dot{\mathbf{r}}) \quad (3.1a)$$

$$\mathbf{r}(t) = [x \ y \ z \ \phi \ \theta \ \psi] = [E \ \Upsilon]^T \quad (3.1b)$$

Solving for the kinetic and potential energies respectively results in;

$$\mathcal{L} = \frac{1}{2} V^T . m_b . V + \frac{1}{2} \dot{\Upsilon}^T . \mathbb{I}_b . \dot{\Upsilon} - mgz \quad (3.2)$$

Noting that  $\mathbb{I}_b$  is w.r.t  $\mathcal{F}^b$  and so, the correct term translated to the inertial frame would actually be;

$$\frac{1}{2} \dot{\Upsilon}^T (\mathbb{R}^T(\Upsilon) \mathbb{I}_B \mathbb{R}(\Upsilon)) \dot{\Upsilon} \quad (3.3)$$

With  $\mathbb{R}^T \mathbb{I}_b \mathbb{R}$  sometimes referred to as the Jacobian, in the context of Euler Lagrange. The famous Lagrange Equation equates the partial derivatives of the Lagrangian to any generalized forces acting

on the system.

$$\frac{\delta}{\delta t} \left( \frac{\delta L}{\delta \dot{q}_i} \right) - \frac{\delta L}{\delta q_i} = \begin{bmatrix} F \\ \tau \end{bmatrix} \quad (3.4)$$

Taking the partial derivatives then stipulates:

$$\begin{bmatrix} F \\ \tau \end{bmatrix} = \frac{1}{2} m_b \frac{\delta}{\delta t} V^2 + \frac{1}{2} \frac{\delta}{\delta t} ((\mathbb{R}^T \mathbb{I}_b \mathbb{R}) \dot{\Upsilon}^2) - \frac{\delta}{\delta q_i} (m_b g z) \quad (3.5a)$$

$$= 2 \frac{1}{2} m_b \dot{V} + \frac{1}{2} \left( \frac{\delta}{\delta t} (\mathbb{R}^T \mathbb{I}_b \mathbb{R}) \dot{\Upsilon} + \mathbb{R}^T \mathbb{I}_b \mathbb{R} \frac{\delta}{\delta t} (\dot{\Upsilon}^2) \right) - m_b g \quad (3.5b)$$

$$= m_b \ddot{E} + \frac{1}{2} \left( (\dot{\mathbb{R}}^T \mathbb{I}_b \mathbb{R} + \mathbb{R}^T \mathbb{I}_b \dot{\mathbb{R}}) \dot{\Upsilon} + 2 \mathbb{R}^T \mathbb{I}_b \mathbb{R} \ddot{\Upsilon} \right) - m_b g \quad (3.5c)$$

$$= m_b \ddot{E} + \frac{1}{2} \left( (\mathbb{S} \mathbb{R})(\omega) \right) \quad (3.5d)$$

method of derivation, derived from conservation of energy theories, is used for presenting the fundamental 6-DOF equations of motion. The

### 3.1.2 Rotation Matrix Peculiarities

### 3.1.3 Quaternion Dynamics

### 3.1.4 The Unwinding Problem

## 3.2 Non-linearities

### 3.2.1 Gyroscopic Torques

### 3.2.2 Coriolis Acceleration

### 3.2.3 Inertial Matrix

## 3.3 Aerodynamics

### 3.3.1 Thrust Forces & Propeller Torques

### 3.3.2 Drag

### 3.3.3 Conning & Flapping

### 3.3.4 Vortex Ring State

## 3.4 Consolidated Model



## Chapter 4

# Control Treatment

### Control Plant & Discussion

#### Control Plant Inputs

#### Model Dependent & Independent Controllers

### 4.1 Attitude Control

#### 4.1.1 The Attitude Control Problem

#### 4.1.2 Quaternion Based Controllers

#### PD Controller

#### Auxilliary Plant Controller

#### PID Controller

#### 4.1.3 Non-linear Controllers

#### Ideal Back-stepping Controller

#### Adaptive Back-stepping Controller

#### Lyupanov Derived Ideal Controller

### 4.2 Position Control

#### 4.2.1 Backstepping Position Controller

### 4.3 Controller Allocation

#### 4.3.1 Non-linear Plant Control Allocation

#### 4.3.2 Pseudo Inverse Allocator

## Chapter 5

# Simulations & Results

### 5.1 Controller Tuning

#### 5.1.1 Partical Swarm Based Optimization

#### 5.1.2 Performance Metric

#### 5.1.3 Global & Local Minima

#### 5.1.4 Fmincon Differences

### 5.2 Simulation Block

### 5.3 State Estimation

### 5.4 Optimized Controller Comparisons

#### 5.4.1 Allocator Performance

#### 5.4.2 Attitude Control Results

#### 5.4.3 Autopilot Outcome

## Chapter 6

# Prototype Flight Results

## Appendix A

# Standard Quadrotor Dynamics

# Appendix B

## Design Bill of Materials

### B.1 Parts List

Part Name	No. Used	Unit Weight[g]
Electronics		
SPRacing F3 Deluxe Flight Controller	1	6
OrangeRx 615X 2.4 GHz 6CH Receiver	1	9.8
Signal Converter SBUS-PPM-PWM	1	5.0
STLink-V2 Debugger	1	N/A
RotorStar Super Mini S-BEC 10A	1	30
128x96" OLED Display	1	N/A
XBee-Pro S1	2	N/A
HobbyWing XRotor 15A Opto ESC	4	10.5
OrangeRX RPM Sensor	4	6
HobbyKing Multi-Rotor Power Distribution Board	1	7.6
Motors		
Corona DS-339MG	8	32
Turnigy DST-700KV Brushlesss DC	4	65
Frame Components		
APM Flight Controller Damping Platform	1	16
HobbyKing SK450 Replacement Arm (2 pcs)	2	N/A
SK450 Extended Landing Skid	1	93
Alloy Servo Arm (FUTABA)	8	N/A
10X18X6 Radial Ball Bearing	8	N/A
80g Damping Ball	32	N/A
Plastic Retainers for Damping Balls	32	N/A
3/5mm Aluminum Prop Adapter	4	N/A
6x4.5 Gemfam 3-Blade Propeller	4	N/A
M3 6mm Hex Nylon Spacer	8	N/A
M3 16mm Hex Nylon Spacer	32	N/A
M3 25mm Nylon Screw	128	N/A
M2.5x10mm Socket Head Cap Screw	36	N/A
M2.5x25mm Socket Head Cap Screw	20	N/A
M2.5 A-Lok Nut	16	N/A

**Table B.1:** Parts List



Technical drawing of a mechanical assembly, showing 14 individual parts (A.1 to H.4) with their dimensions and views.

**Part A.1:** Dimensions include 10.0, 38.17, 1.6, 12.00, 3.00, 1.00,  $\phi 2.50$ ,  $\phi 9.40$ .

**Part A.2:** Dimensions include 14.00, 2.00, 10.00, 2.00,  $\phi 2.50$ , P.C.D  $\phi 157.00$ , R84.00, R73.00,  $\phi 2.80$ , 12.00.

**Part B.1:** Dimensions include 32.13, 2.00, 10.00, 14.00,  $\phi 10.00$ .

**Part B.2:** Dimensions include 2.00, 14.00, 2.00, 10.00, P.C.D  $\phi 157.00$ , R73.00, R84.00, 14.00, 12.00,  $\phi 2.80$ .

**Part C.1:** Dimensions include 10.00, 2.00, 3.00, 3.00, 15.00, 14.00, 46.00, R3.00, 9.00,  $\phi 3.00$ , 38.00.

**Part C.2:** Dimensions include 2.00, 10.00, 5.50, P.C.D  $\phi 197.50$ , 3.00, 12.00, R90.50,  $\phi 2.80$ , R107.00.

**Part D.1:** Dimensions include 1.25, 7.00, R105.05, R7.90, R12.90, R11.00, 3.00, 1.25, 35°, 12.10, 1.95, R90.50, P.C.D  $\phi 197.50$ .

**Part D.2:** Dimensions include 2.00, 13.00, 5.14, 55,  $\phi 25.40$ ,  $\phi 22.40$ ,  $\phi 19.40$ ,  $\phi 15.00$ , 3.00, 23.00, 21.40, 23.00,  $\phi 15.00$ .

**Part D.3:** Dimensions include 2.00, 13.00, 5.14, 55,  $\phi 25.40$ ,  $\phi 22.40$ ,  $\phi 19.40$ , 3.00, 23.00, 21.40, 23.00,  $\phi 15.00$ .

**Part D.4:** Dimensions include 4.00, 2.00, 55,  $\phi 25.40$ ,  $\phi 22.40$ ,  $\phi 19.40$ ,  $\phi 15.00$ , 3.00, 23.00, 21.40, 23.00,  $\phi 15.00$ .

**Part E.1:** Dimensions include 6.50, 6.50, 13.00, 25.00, 7.80,  $\phi 1.00$ , 6.50, 18.50, 32.70, 24.90,  $\phi 3.20$ .

**Part E.2:** Dimensions include 6.50, 6.50, 13.00, 25.00, 7.80,  $\phi 1.00$ , 14.30, 6.50, 18.50, 32.70, 24.90,  $\phi 3.20$ .

**Part F.1:** Dimensions include 38.00, 14.00, 3.00, 18.00,  $\phi 10.00$ , 14.00, 3.00.

**Part F.2:** Dimensions include 5.50, 2.00, R90.50, P.C.D  $\phi 197.50$ ,  $\phi 2.80$ , 12.00, R107.00, 10.00, 14.00, 3.00.

**Part F.3:** Dimensions include 5.50, 3.00, 10.00, 6.50, R90.50, P.C.D  $\phi 197.50$ ,  $\phi 2.80$ , 12.00, R107.00, 14.00, 3.00.

**Part G.1:** Dimensions include 1.50, 4.50, R12.70, R10.70, R7.50,  $\phi 2.80$ , 28.73, 13.16, 18.58, R3.00.

**Part G.2:** Dimensions include 1.50, 4.50, R12.70, R10.70, R7.50,  $\phi 2.80$ , 28.73, 13.16, 18.58, R3.00.

**Part H.1:** Dimensions include 6.50, 6.50, 13.00, 25.00, 7.80,  $\phi 1.00$ , 6.50, 18.50, 32.70, 24.90,  $\phi 3.20$ .

**Part H.2:** Dimensions include 6.50, 6.50, 13.00, 25.00, 7.80,  $\phi 1.00$ , 14.30, 6.50, 18.50, 32.70, 24.90,  $\phi 3.20$ .

**Part H.3:** Dimensions include 4.00, 2.00, 55,  $\phi 25.40$ ,  $\phi 22.40$ ,  $\phi 19.40$ ,  $\phi 15.00$ , 3.00, 23.00, 21.40, 23.00,  $\phi 15.00$ .

**Part H.4:** Dimensions include 4.00, 2.00, 55,  $\phi 25.40$ ,  $\phi 22.40$ ,  $\phi 19.40$ ,  $\phi 15.00$ , 3.00, 23.00, 21.40, 23.00,  $\phi 15.00$ .

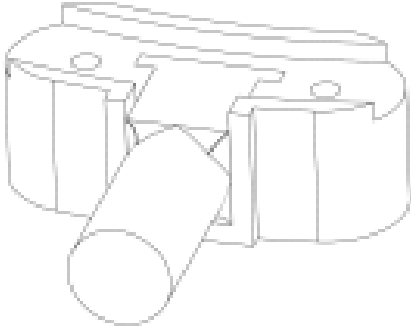
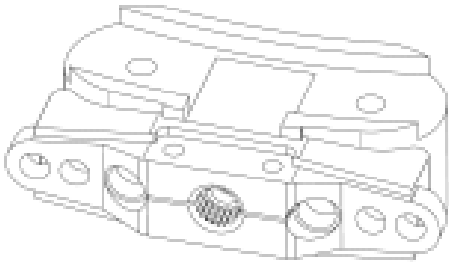
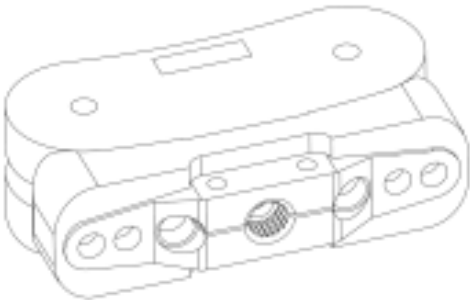

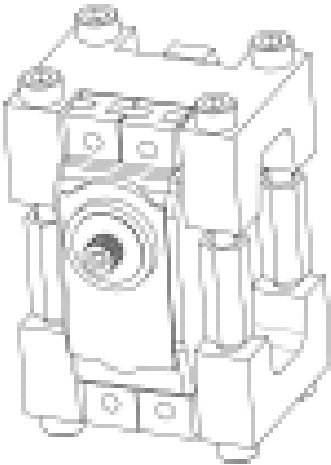
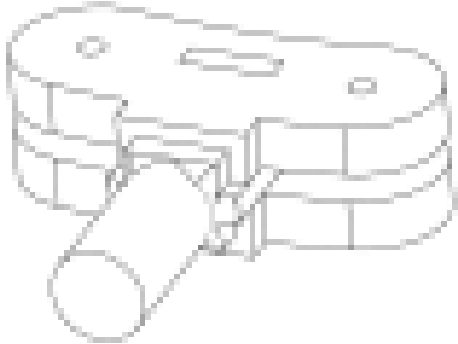
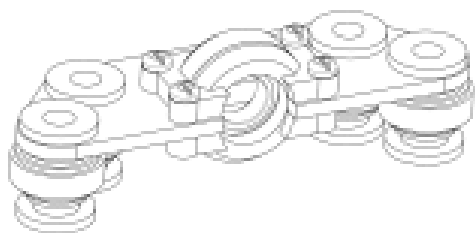
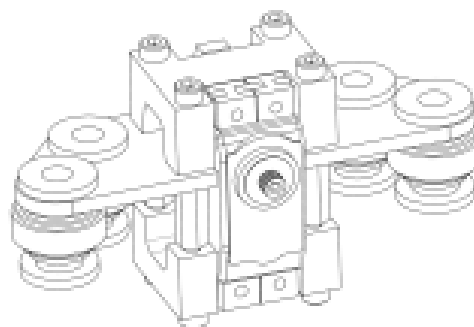
Bracket Assemblies 2	
 <p><b>Figure B.1:</b> Bearing Bracket Inner Ring Assembly Parts: A.1, A.2</p>	 <p><b>Figure B.2:</b> Servo Bracket Inner Ring Assembly Parts: B.1, B.2, M3 Servo Horn</p>
 <p><b>Figure B.3:</b> Servo Bracket Middle Ring Assembly Parts: C.1, C.2, C.3, M3 Servo Horn</p>	 <p><b>Figure B.4:</b> Bearing Holder Middle Ring Assembly Parts: D.1, D.2, D.3, D.4, 18-10 Bearing</p>
 <p><b>Figure B.5:</b> Servo Mount Middle Ring Assembly Parts: E.1, E.2, Corona Servo &amp; Fasteners</p>	 <p><b>Figure B.6:</b> Bearing Shaft Middle Ring Assembly Parts: F.1, F.2, F.3</p>

Table B.3: Inner & Middle Ring Assemblies

## Bracket Assemblies 2



**Figure B.7:** Bearing Holder Damping Assembly  
Parts: G.1, G.2, G.3, G.4, 18-10 Bearing, 80g  
Damping Balls, Bearing Holder Damping Bracket

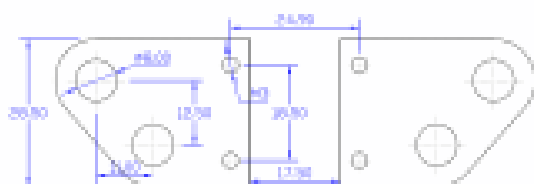


**Figure B.8:** Servo Mount Damping Assembly  
Parts: H.1, H.2, Corona Servo & Fasteners, 80g  
Damping Balls, Servo Mount Damping Bracket

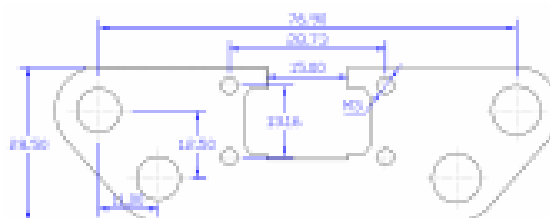
**Table B.4:** Damping Assemblies

---

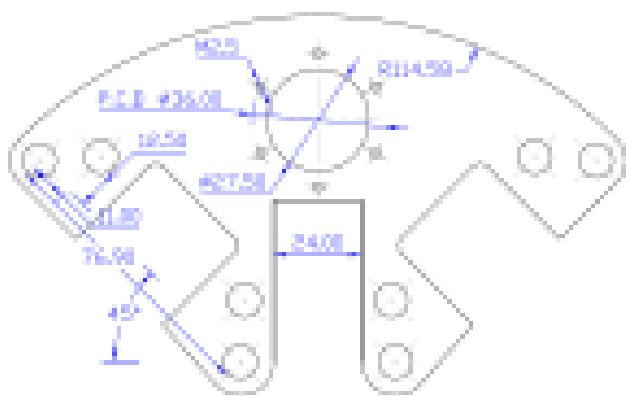
## Laser Cut Brackets



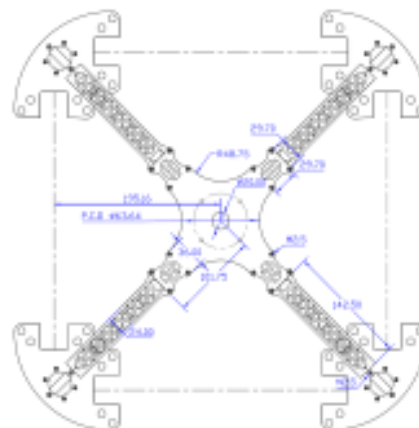
**Figure B.9:** Servo Mount Damping Bracket



**Figure B.10:** Bearing Holder Damping Bracket



**Figure B.11:** Arm Mount Damping Bracket



**Figure B.12:** Frame Brackets

**Table B.5:** Laser Cut Damping Brackets

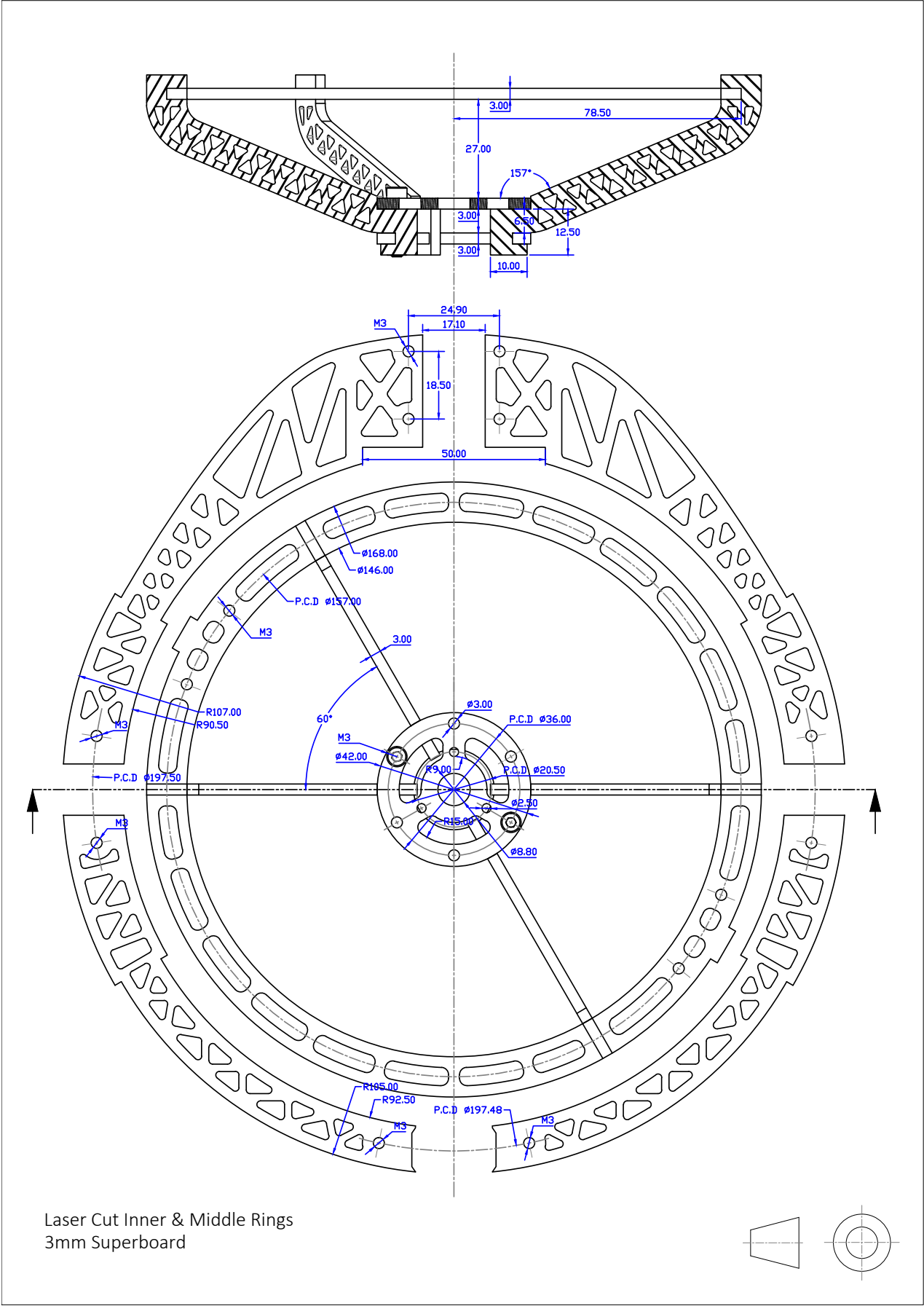


Table B.6: Laser Cut Parts

The diagram illustrates a complex PCB layout for an STM32F303I microcontroller-based system. The central component is the STM32F303I microcontroller, which is connected to various peripheral components and interfaces. Key components and connections include:

- Microcontroller (STM32F303I):** The central processing unit, with pins connected to various peripherals and power/ground planes.
- MPU6050:** A digital motion sensor connected to the microcontroller via I2C (SCL/PB6, SDA/PB7) and power (VCC, GND).
- N25Q064A:** A 64Kbit SPI flash memory connected to the microcontroller via SPI (CS, SCK, MISO, MOSI) and power (VCC, GND).
- CP2102:** A USB-to-UART bridge chip connected to the microcontroller's UART pins (TX, RX, GND, VCC) and a USB port.
- UART Modules:** Several UART modules (UART1, UART2, UART3, UART4) are connected to the microcontroller's UART pins and external UART pins.
- Power and Ground:** The board features a 3.3V power plane and a ground plane. Power is supplied to various components via 3.3V and GND pins.
- Connectors:** The board includes a micro-USB port, an I2C connector, a UART connector, and a 3.3V LED strip connector.
- Other Components:** The board also includes a buzzer (BUZZER), a 3.3V LED strip, and various passive components like resistors and capacitors.

The layout is highly detailed, showing the physical placement of components, the routing of signals, and the connection to various external devices and power sources.

**Figure B.13:** F3 Deluxe Flight Controller Hardware Schematic

## Appendix C

# System ID Test Data

### C.1 Servo Data

## C.2 Cobra CM2208-200KV

Cobra CM-2208/20 Motor Propeller Data										
Magnets 14-Pole	Motor Wind 20-Turn Delta	Motor Kv 2000 RPM/Volt		No-Load Current Io = 0.77 Amps @ 10v		Motor Resistance Rm = 0.076 Ohms		I Max 20 Amps	P Max (3S) 220 W	
Stator 12-Slot	Outside Diameter 27.7 mm, 1.091 in.	Body Length 24.0 mm, 0.945 in.		Total Shaft Length 45.2 mm, 1.780 in.		Shaft Diameter 3.17 mm, 0.125 in.		Motor Weight 44.2 gm, 1.56 oz		
Test Data From Sample Motor		Input Io Value	6.0 V 0.59 A	8.0 V 0.67 A	10.0V 0.77 A	12.0V 0.87 A	Measured Kv value 1988 RPM/Volt @ 10v	Measured Rm Value 0.076 Ohms		
Prop Manf.	Prop Size	Li-Po Cells	Input Voltage	Motor Amps	Input Watts	Prop RPM	Pitch Speed in MPH	Thrust Grams	Thrust Ounces	Thrust Eff. Grams/W
APC	5.25x4.75-E	3	11.1	13.34	148.1	17,507	78.7	451	15.91	3.05
APC	5.5x4.5-E	3	11.1	13.67	151.7	17,388	74.1	456	16.08	3.01
APC	6x4-E	3	11.1	14.87	165.1	17,003	64.4	630	22.22	3.82
APC	7x4-SF	3	11.1	21.82	242.2	13,985	53.0	840	29.63	3.47
APC	7x5-E	3	11.1	24.02	266.6	13,272	62.8	797	28.11	2.99
FC	5x4.5	3	11.1	8.66	96.1	19,061	81.2	428	15.10	4.45
FC	5x4.5x3	3	11.1	12.38	137.4	17,825	76.0	534	18.84	3.89
FC	6x4.5	3	11.1	15.47	171.7	16,792	71.6	721	25.43	4.20
GemFan	5x3	3	11.1	6.67	74.0	19,801	56.3	374	13.19	5.05
HQ	5x4	3	11.1	7.13	79.1	18,182	68.9	373	13.16	4.71
HQ	5x4x3	3	11.1	9.25	102.7	17,401	65.9	449	15.84	4.37
HQ	5x4.5-BN	3	11.1	11.17	124.0	16,902	72.0	487	17.18	3.93
HQ	6x3	3	11.1	7.34	81.5	18,128	51.5	419	14.78	5.14
HQ	6x4.5	3	11.1	13.53	150.2	16,206	69.1	645	22.75	4.29
HQ	6x4.5x3	3	11.1	17.60	195.4	15,137	64.5	762	26.88	3.90
HQ	7x4	3	11.1	20.71	229.9	14,250	54.0	850	29.98	3.70
HQ	7x4.5	3	11.1	20.31	225.4	14,351	61.2	865	30.51	3.84
Prop Manf.	Prop Size	Li-Po Cells	Input Voltage	Motor Amps	Input Watts	Prop RPM	Pitch Speed in MPH	Thrust Grams	Thrust Ounces	Thrust Eff. Grams/W
APC	5.25x4.75-E	4	14.8	17.29	255.9	20,560	92.5	603	21.27	2.36
APC	5.5x4.5-E	4	14.8	17.87	264.5	20,436	87.1	635	22.40	2.40
APC	6x4-E	4	14.8	20.15	298.2	19,829	75.1	837	29.52	2.81
FC	5x4.5	4	14.8	10.89	161.2	22,511	95.9	588	20.74	3.65
FC	5x4.5x3	4	14.8	16.43	243.2	20,828	88.8	718	25.33	2.95
FC	6x4.5	4	14.8	20.09	297.3	19,809	84.4	998	35.20	3.36
HQ	4x4.5-BN	4	14.8	10.45	154.7	22,661	96.6	477	16.83	3.08
HQ	5x3	4	14.8	6.88	101.8	23,580	67.0	442	15.59	4.34
HQ	5x4	4	14.8	10.22	151.3	22,739	86.1	589	20.78	3.89
HQ	5x4x3	4	14.8	13.26	196.2	21,763	82.4	710	25.04	3.62
HQ	5x4.5-BN	4	14.8	16.10	238.3	20,899	89.1	744	26.24	3.12
HQ	6x3	4	14.8	11.06	163.7	22,512	64.0	679	23.95	4.15
HQ	6x4.5	4	14.8	19.62	290.4	19,948	85.0	982	34.64	3.38

Figure C.1: Official Test Results for Cobra Motors

## Appendix D

### Full Equations

#### D.1 Inertias

$$\approx \begin{bmatrix} 3613.144 & 0.025 & 406.81 \\ 0.025 & 9774.160 & 0.4626 \\ 406.81 & 0.4626 & 12650.72 \end{bmatrix} \quad (\text{D.1a})$$

$$\begin{bmatrix} 0 & -0.249s\lambda - 0.276c\lambda & 0.249c\lambda - 0.276s\lambda \\ -0.249s\lambda - 0.276c\lambda & -0.448s2\lambda - 2142.67s\lambda + 983c\lambda & 983s2\lambda - 2142.67s\lambda + 0.448c2\lambda \\ 0.249c\lambda - 0.276s\lambda & 983s2\lambda - 2142.67s\lambda + 0.448c2\lambda & 1967.497s\lambda + 1070.88c2\lambda + 0.448s2\lambda \end{bmatrix} \quad (\text{D.1b})$$

$$= \begin{bmatrix} 814c_\eta s_\eta + 3613c_\eta^2 + 11580s_\eta^2 + 2142c_\lambda^2 s_\eta^2 + 1967s_\eta^2 s_\lambda^2 + 2c_\lambda s_\eta^2 s_\lambda - c_\eta s_\eta s_\lambda \\ 2c_\lambda^2 s_\lambda - s_\lambda - 175c_\lambda s_\eta s_\lambda \\ 4967s_{2\eta} + 814c_\eta^2 - c_\eta^2 s_\lambda + 175c_\eta c_\lambda^2 s_\eta + 2c_\eta c_\lambda s_\eta s_\lambda \\ 2c_\lambda^2 s_\eta - s_\eta - 175c_\lambda s_\eta s_\lambda \\ 10933 - 175c_\lambda^2 - s_{2\lambda} \\ 2c_\eta c_\lambda^2 - c_\eta - 175c_\eta c_\lambda s_\lambda \\ 4967s_{2\eta} + 814c_\eta^2 - c_\eta^2 s_\lambda + 175c_\eta c_\lambda^2 s_\eta + 2c_\eta c_\lambda s_\eta s_\lambda - 407 \\ 2c_\eta c_\lambda^2 - c_\eta - 175c_\eta c_\lambda s_\lambda \\ 9933c_\eta^2 - 814c_\eta s_\eta + 175c_\eta^2 c_\lambda^2 + 2c_\eta^2 c_\lambda s_\lambda + c_\eta s_\eta s_\lambda \end{bmatrix} \quad (\text{D.1c})$$

$$= \mathbb{R}_Z \begin{bmatrix} c_{\eta_i} & 0 & s_{\eta_i} \\ 0 & 1 & 0 \\ -s_{\eta_i} & 0 & c_{\eta_i} \end{bmatrix} (\mathbb{I}_{M'_i}) \begin{bmatrix} c_{\eta_i} & 0 & -s_{\eta_i} \\ 0 & 1 & 0 \\ s_{\eta_i} & 0 & c_{\eta_i} \end{bmatrix} \mathbb{R}_Z^{-1} \quad (\text{D.1d})$$



# Bibliography

- [1] Yazan Al-Rihani. *Development of a dual axis tilt rotorcraft uav: Design, prototyping and control.*, volume 1. Cranfield University: School of Engineering, 2012.
- [2] N. Amiri, A. Ramirez-Serrano, and Davies R. Modelling of opposed lateral and longitudinal tilting dual-fan unmanned aerial vehicle. *International Federation of Automatic Control*, pages 2054–2059, September 2011.
- [3] APMCopter. Arducopter main page. Website: <http://www.arducopter.co.uk/>, 6 2016. Arducopter (APM) Official Website.
- [4] E. Balasubramanian and R. Vasantharaj. Dynamic modelling and control of quadrotor. *International Journal of Engineering and Technology*, pages 63–39, February 2013.
- [5] M. Bangura and R. Mahony. Non-linear dynamic modelling for high performance control of a quadrotor. In *Australasian Conference on Robotics and Automation, Victoria University of Wellington*. Victoria University of Wellington, 12 2012. Published in Conference Proceedings.
- [6] Mohd Ariffanan Basri, Abdul R. Husain, and Kumeresan A. Danapalasingam. Intelligent adaptive backstepping control for mimo uncertain non-linear quadrotor helicopter systems. *Institute of Measurement Control Transactions*, pages 1–17, 2014.
- [7] BetaFlight. Betaflight fc4 repo, 2016. Forked from the CleanFlight repo.
- [8] Charles Blouin and Eric Lantagne. Pitch control on an oblique active tilting bi-rotor. *International Conference on Unmanned Aircraft Systems*, pages 791–799, May 2014.
- [9] R. Bodrany, W. Steyn, and M. Crawford. In-orbit estimation of the inertia matrix and thruster parameters of uosat-12. In *Conference on Small Satellites*, volume 14, pages 1–11. American Institute of Aeronautics and Astronautics, 2000.
- [10] Hossein Bolandi, Mohammed Rezaei, Rezo Mohsenipour, Hossein Nemati, and Seed Majid Smailzadeh. Attitude control of a quadrotor with optimized pid. *Intelligent Control and Automation*, pages 335–342, August 2013.
- [11] S. Bouabdallah and R. Siegwart. Full control of a quadrotor. *IEEE International Conference on Intelligent Robots and Systems*, pages 153–158, 11 2007. Written for Autonomous Systems Lab at Swiss Federal Institute of Technology.
- [12] Samir Bouabdallah, Andre Noth, and Roland Siegward. Pid vs lq control techniques applies to an indoor micro quadrotor. *IEEE International Conference on Intelligent Robots and Systems*, pages 2451–2456, 9 2004.
- [13] J. Brandt and M. Selig. Propeller performance data at low reynolds numbers. *American Institute of Aeronautics and Astronautics Sciences Meeting, 49th*, pages 1–18, January 2011.
- [14] Jian Chen, Aman Behal, and Darren M. Dawson. Adaptive output feedback control for a class of mimo nonlinear systems. In *Proceedings of the American Control Conference*, pages 5300–5306, Minneapolis, Minnesota, US, 6 2006. American Control Conference.

- [15] Arindam B. Chowdhury, Anil Kulhare, and Guarav Raina. A generalized control method for tilt-rotor uav stabilization. *IEEE International Conference on Cyber Technology in Automation, Control and Intelligent Systems*, pages 309–314, May 2012.
- [16] Dominic Clifton. Spracing f3 deluxe flight controller, 2015.
- [17] R.F. de Olivera, F.T. de Salvi, and E.M. Belo. Dynamic modelling, simulation and control of an autonomous quadcopter aircraft. *International Congress of Mechanical Engineering*, pages 1–9, November 2009.
- [18] Innov8tive Designs. Cobra cm2208/2000 motors, 2016.
- [19] Chen Diao, Bin Xian, Qiang Yin, Wei Zeng, Haotao Li, and Yungao Yang. A nonlinear adaptive control approach for quadrotor uavs. In *Asian Control Conference Proceedings*, volume 8, pages 223–228, Kaohsiung, Taiwan, 5 2011. Asian Control Conference.
- [20] DJI Drones. Dji inspire one, 2016.
- [21] DJI Drones. Dji phantom, 2016.
- [22] Honeywell Solid State Electronics. Hmc5833 magnetometer datasheet. Advanced Information Data Sheet, 10 2010. Available From: <https://strawberry-linux.com/pub/HMC5883L.pdf>.
- [23] Emil Fresk and George Nikolakopoulos. Full quaternion based attitude control for a quadrotor. *European Control Conference*, pages 3864–3869, 6 2013.
- [24] Pau. S Gasco. *Development of a Dual Axis Tilt Rotorcraft UAV: Modelling, Simulation and Control*, volume 1. Cranfield University: School of Engineering, 2012.
- [25] HiSystems GmbH. Mikrokopter quadroxl, 2016.
- [26] Basile Graf. Quaternions and dynamics. Publication for Mathematics - Dynamical Systems, 2 2007.
- [27] Gary R. Gress. Lift fans as gyroscopes for controlling compact vtol air vehicles: Overview and development status of oblique active tilting. In *American Helicopter Society Annual Forum*, volume 63, Virginia Beach, 5 2007. American Helicopter Society, American Helicopter Society Inc. Forum Proceedings.
- [28] Gary R. Gress. *Passive Stabilization of VTOL Aircraft Having Obliquely Tilting Propellers*. University of Calgary, Department of Mechanical Engineering, Calgary, Alberta, 2014.
- [29] Karsten Groekatthfer and Zizung Yoon. Introudction into quaternions for spacecraft attitude representation. *Technical University of Berlin: Department of Astronautics and Aeronatuics*, pages 1–16, May 2012.
- [30] N. Guenard, T. Hamel, and V. Moreau. Dynamic modelling and control strategy for an x4-flyer. *International Conference on Control and Automation*, pages 141–146, June 2005.
- [31] HobbyKing. Orangerx rpm sensor, 2016.
- [32] HobbyKing. Rotorstar super mini s-bec, 2016.
- [33] HobbyKing. Signal converter module sbus-ppm-pwm, 2016.
- [34] HobbyKing.com. Hobby king: The ultimate hobby experience, 2016.

- [35] G. Hoffmann, H. Huang, S. Waslander, and C. Tomlin. Quadrotor helicopter flight dynamics and control: Theory and experiment. In *Guidance, Navigation and Control Conference and Exhibit*, pages 1–19, Hilton Head, South Carolina, 8 2010. American Institute of Aeronautics and Astronautics, American Institute of Aeronautics and Astronautics. Derivation of advanced aerodynamic affects on STARMAC Quadrotor Prototype.
- [36] InvenSense Inc. Mpu6050 6-axis gyroscope/accelerometer datasheet. Product Specification Data Sheet, 8 2013. Available From:[https://www.cdiweb.com/datasheets/invensense/MPU-6050\\_DataSheet\\_V3%204.pdf](https://www.cdiweb.com/datasheets/invensense/MPU-6050_DataSheet_V3%204.pdf).
- [37] Digi International. Xbee/xbee pro rf modules. Technical Data Sheet, 9 2009. Available From:<https://www.sparkfun.com/datasheets/Wireless/Zigbee/XBee-Datasheet.pdf>.
- [38] W. Jia, Z. Ming, Y. Zhiwei, and L. Bin. Adaptive back-stepping lpv control of satellite attitude maneuvers with sum of squares. In *World Congress on Intelligent Control and Automation*, volume 8, pages 1747–1752. IEEE, 7 2010.
- [39] Tor A. Johansen and Thor I. Fossen. Control allocation - a survey. *Automatica*, 45:10871103, 11 2012. Prepared for: Department of Engineering Cybernetics - Norwegian University of Science and Technology.
- [40] Farid Kendoul, Isabelle Fantoni, and Rogelio Lozano. Modeling and control of a small autonomous aircraft having two tilting rotors. *IEEE Conference on Decision and Control*, pages 8144–8149, December 2005.
- [41] P. Krishnamurthy and F. Khorrami. Adaptive backstepping and theta-d based controllers for a tilt-rotor aircraft. *Mediterranean Conference on Control and Automation*, pages 540–545, June 2011.
- [42] Raymond Kristiansen and Per J. Nicklasson. Satellite attitude control by quaternion-based back-stepping. *American Control Conference*, N/A:907–912, 6 2005. Published by Department of Computer Science, Electrical Engineering and Space Technology; Narvik University College.
- [43] Jack B. Kuipers. *Quaternions and Rotation Sequences: A Prier with Aplication to Orbital Aerospace and Virtual Reality*, pages 127–143. Princeton University Press, September 2002. Used for Quaternion and Rotation Matrix reference.
- [44] Peter Lambert. Nakazawa, banton and jin, bai x. Technical Report N/A, Computer and Electrical Engineering: University of Victoria, Victoria, Canada, 12 2013.
- [45] Prof Allan J. Laub. The moore-penrose pseudo inverse. UCLA Math33A Course Content, UCLA, Los Angeles, 3 2008. Course Notes cited from <http://www.math.ucla.edu/~laub/33a.2.12s/mpppseudoinverse.pdf>.
- [46] Jang-Ho Lee, Byoung-Mun Min, and Eung-Tai Kim. Autopilot design of tilt-rotor uav using particle swarm optimization method. *International COnference on Control, Automation and Systems*, pages 1629–1633, October 2007.
- [47] LibrePilot. Openpilot/librepilot wiki. Website: <http://opwiki.readthedocs.io/en/latest/index.html>, 5 2016. Information wiki page for LibrePilot/OpenPilot firmware.
- [48] Hyon Lim, Jaemann Park, Daewon Lee, and H.J. Kim. Build your own quadrotor. *IEEE ROBOTICS & AUTOMATION MAGAZINE*, pages 33–45, 9 2012. Publication on Opensource Autopilot systems.
- [49] SteadiDrone PTY LTD. Steadidrone home, 2016.

- [50] Teppo Luukkonen. Modelling and control of a quadcopter. Master's thesis, Aalto University: School of Science, Espoo, Finland, 8 2011. Independent research project in applied mathematics.
- [51] Tarek Madani and Abdelaziz Benallegue. Backstepping control for a quadrotor helicopter. *International Conference on Intelligent Robots and Systems*, pages 3255–3260, October 2006.
- [52] I. Mandre. Rigid body dynamics using euler's equations, rungekutta and quaternions, 2 2006.
- [53] Carlos J. Mantas and Jose M. Puche. Artificial neural networks are zero-order tsk fuzzy systems. In *IEEE Transactions on Fuzzy Systems*, volume 16, pages 630–644, 6 2008.
- [54] Christopher G. Mayhew, Ricardo G. Sanfelice, and Andrew R. Teel. On quaternion based attitude control and the unwinding phenomenon. *American Control Conference*, pages 299–304, June 2011.
- [55] Ashfaq A. Mian and Wang Daoboo. Modelling and backstepping-based nonlinear control of a 6dof quadrotor helicopter. *Chinese Journal of Aeronautics*, 21:261–268, 3 2008. Simulated Backstepping Control.
- [56] Svein Rivli Napsholm. Prototype of a tiltrotor helicopter. Master's thesis, Norwegian University of Science and Technology: Department of Engineering Cybernetics, Norway, 1 2013.
- [57] A. Nemati and M. Kumar. Modeling and control of a single axis tilting quadcopter. *American Control Conference*, pages 3077–3082, June 2014.
- [58] Kenzo Nonami, Farid Kendoul, Satoshi Suzuki, Wei Wang, and Daisuke Nakazawa. *Autonomous Flying Robots: Unmanned Aerial Vehicles and Micro Aerial Vehicles*, chapter 2, pages 44–48. Springer Japan, 1 edition, 2010. References to Cyclic-Pitch Control relevant subsections.
- [59] Gustavo P. Oliveira. Quadcopter civil applications. Master's thesis, Informatics and Computer Engineering: University of Portugal, Portugal, 2 2014.
- [60] OrangeRx. Orangerx r615x receiver. User Manual, 10 2014. Available From:<http://www.hobbyking.com/hobbyking/store/uploads/672761531X1606554X18.pdf>.
- [61] Christos Papachristos, Kostas Alexis, and Anthony Tzes. Design and experimental attitude control of an unmanned tilt-rotor aerial vehicle. *International Conference on Advanced Robotics*, pages 465–470, June 2011.
- [62] Parth N. Patel, Malav A. Patel, Rahul M. Faldu, and Yash R. Dave. Quadcopter for agricultural surveillance. In *Advance in Electronic and Electrical Engineering*, volume 3, India, 2013.
- [63] J. Peraire and S. Widnall. 3d rigid body dynamics: Euler angles. Lecture notes for Dynamics Course, 2009. Dynamics course notes, fall 2007.
- [64] J. Peraire and S. Widnall. 3d rigid body dynamics: The inertia tensor. Lecture notes for Dynamics Course, 2009. Dynamics course notes, fall 2007.
- [65] D. Peters. Eighth amendment of the civil aviation regulations. Government Gazette Notice, 5 2015. In Amendment to the Civil Aviation Act, 2009 (Act No.13 of 2009).
- [66] Jean-Baptiste Pomet and Laurent Praly. Adaptive nonlinear regulation: Estimation from the lyapunov equation. In *IEEE Transactions on Automatic Control*, volume 37, pages 729–740. IEEE, 6 1992.
- [67] P. Pounds, R. Mahony, P. Hynes, and J. Roberts. Design of a four-rotor aerial robot. *Australasian Conference on Robotics and Automation*, pages 145–150, November 2002.
- [68] Dimitry Prof. Garanin. Rotational motion of rigid bodies. Analytical Dynamics Course Notes, 11 2008. Content for City University of New York.

- [69] Beard Randal. Quadrotor dynamics and control. Report, Brigham Young University, 2 2008. Part of the Electrical and Computer Engineering Commons.
- [70] O. Rawashdeh, H.C. Yang, R. AbouSleiman, and B. Sababha. Microraptor: A low cost autonomous quadrotor system. *International Design Engineering Technical Conferences & Computers and Information in Engineering Conference*, pages 1–8, August 2009.
- [71] Anastasia Razinkove, Igor Gaponov, and Hyun-Chan Cho. Adaptive control over quadcopter uav under disturbances. *International Conference on Control, Automation and Systems*, pages 386–390, October 2014.
- [72] M.K. Rwigema. Propeller blade element momentum theory with vortex wake deflection. *International Congress of the Aeronautical Sciences, 27th*, pages 1–9, January 2010.
- [73] M. Ryll, H. Bulthoff, and P. Robuffo Giordano. Modelling and control of a quadrotor uav with tilting propellers. *IEEE International Conference on Robotics and Automation*, pages 4606–4613, May 2012.
- [74] M. Ryll, H. Bulthoff, and P. Robuffo Giordano. First flight tests of a quadrotor uav with tilting propellers. *IEEE International Conference on Robotics and Automation*, pages 295–302, May 2013.
- [75] A. Sanchez, J. Escareo, O. Garcia, and R. Lozano. Autonomous hovering of a noncyclic tiltrotor uav: Modeling, control and implementation. *The International Federation of Automatic Control*, pages 803–808, July 2008.
- [76] Puneet Singla, Daniele Mortari, and John L. Junkins. How to avoid singularity when using euler angles? *Advances in the Astronautical Sciences*, pages 1409–1426, January 2005.
- [77] Measurement Speacalties. Ms5611 barometric pressure sensor. Technical Data Sheet, 10 2012. Available From:[http://www.amsys.info/sheets/amsys.en.ms5611\\_01ba03.pdf](http://www.amsys.info/sheets/amsys.en.ms5611_01ba03.pdf).
- [78] STMicroElectronics. St-link/v2 in circuit debugger/programmer for stm32.
- [79] STMicroElectronics. Rm0316 reference manual. Online Micro-Controller Reference Manual, 3 2016. Available From:[http://www.st.com/content/st\\_com/en/products/microcontrollers/stm32-32-bit-arm-cortex-mcus/stm32f3-series/stm32f303.html?querycriteria=productId=LN1531](http://www.st.com/content/st_com/en/products/microcontrollers/stm32-32-bit-arm-cortex-mcus/stm32f3-series/stm32f303.html?querycriteria=productId=LN1531).
- [80] Abdelhamid Tayebi and Stephen McGilvray. Attitude stabilization of a vtol quadrotor aircraft. *IEEE Transactions on Control Systems Technology*, pages 562–571, May 2006.
- [81] Stephen T. Thornton and Jerry B. Marion. *Classical Dynamics of Particles and Systems*, chapter 7, pages 228–289. Thompson Brooks/Cole, 5 edition, 2003.
- [82] John Ting-Yung Wen and Kenneth Kreutz-Delgado. The attitude control problem. *IEEE Transactions on Automatic Control*, pages 1148–1162, October 1991.
- [83] David Tong. Lagrange formalism. Lectures of Classic Dynamics, Course Notes, 2005. Classical Mechanics Notes.
- [84] P. Tsiotras, M. Corless, and J.m Longuski. A novel approach to the attitude control of axisymmetric spacecraft. *Automatica*, 31:1099–1112, 3 1995. Control Automatica, Printed in Great Britan.
- [85] Ultimaker. Ultimaker v2+ product page, 2016.
- [86] E. van Kampen and M. M. van Paassen. Ae4301: Automatic flight control system design. Delft Centre for Systems and Control; MSc Notes, 1 2008. Course Notes cited from: <http://aerostudents.com/master/advancedFlightControl.php>.

- [87] Ronny Votel and Doug Sinclair. Comparison of control moment gyros and reaction wheels for small earth-observing satellites. In *Conference on Small Satellites*, volume 26, pages 1–7. Utah State University, 8 2012. Open access on AIAA conference website.
- [88] Tao Wang, Tao Zhao, Du Hao, and Mingxi Wang. Transformable aerial vehicle, 09 2014.
- [89] X. Xiaozhu, L. Zaozhen, and C. Weining. Intelligent adaptive backstepping controller design based on the adaptive particle swarm optimization. *Chinese Control and Decision Conference*, pages 13–17, September 2009.
- [90] Song Xin and Zou Zaojian. A fuzzy sliding mode controller with adaptive disturbance approximation for an underwater robot. In *International Asia Conference on Informatics in Control, Automation and Robotics*, volume 2, pages 50–53, 10 2010.